High Density Domain-Focused CRISPR Screens Reveal Novel Epigenetic Regulators of *HOX/MEIS* Activation in Acute Myeloid Leukemia

Karina Barbosa[1*], Anagha Deshpande[1*], Marlenne Perales[1], Ping Xiang[2], Rabi Murad[1], Anna Minkina[3], Neil Robertson[4], Fiorella Schischlik[5], Xue Lei[1], Younguk Sun[1], Adam Brown[6], John G. Doench[6], R. Keith Humphries[2], Eytan Ruppin[5], Jay Shendure[3], Prashant Mali[7], Peter D Adams[1], and Aniruddha J. Deshpande[1]

[1]Sanford Burnham Prebys Medical Discovery Institute, La Jolla, CA 92037

2British Columbia Cancer Agency, Vancouver, BC, V5Z 1L3, Canada.

[3] Department of Genome Sciences, University of Washington, Seattle, WA, USA

[4] Beatson Institute for Cancer Research and the University of Glasgow, Glasgow, UK.

[5] Cancer Data Science Laboratory, Center for Cancer Research, National Cancer Institute, National Institutes of Health, Bethesda, MD, 20892, USA.

[6] Broad Institute of Harvard and MIT, Cambridge, MA, USA.

[7] Department of Bioengineering, University of California, San Diego, San Diego, CA 92093, USA

***Equal contribution**

Corresponding author: Aniruddha Deshpande, PhD, Tumor Initiation and Maintenance Program, Sanford Burnham Prebys Medical Discovery Institute, La Jolla, USA, 92037

Email: adeshpande@sbpdiscovery.org

Running title: SGF29 as a Novel Target in AML

Conflict of interest statement: The authors declare no competing interests or conflicts of interest related to this work.

ABSTRACT

Aberrant expression of stem-cell-associated genes is a common feature in acute myeloid leukemia (AML) and is linked to leukemic self-renewal and therapy resistance. Using AF10-rearranged leukemia as a prototypical example displaying a recurrent "*stemness*" network activated in AML, we screened for chromatin regulators that sustain aberrant activation of these networks. We deployed a CRISPR-Cas9 screen with a bespoke domain-focused library and identified several novel chromatin-modifying complexes as regulators of the TALE domain transcription factor MEIS1, a key leukemia stem cell (LSC)-associated gene. CRISPR droplet sequencing revealed that many of these MEIS1 regulators, controlled the transcription of several AML oncogenes. In particular, we identified a role for the Tudor-domain containing chromatin reader protein SGF29 in the transcription of key AML oncogenes. Furthermore, SGF29 deletion impaired leukemogenesis in models representative of multiple AML subtypes. Thus, our studies reveal a novel role for SGF29 as a non-oncogenic dependency in AML and identify the SGF29 Tudor domain as an attractive target for drug discovery.

STATEMENT OF SIGNIFICANCE

Screening for regulators of "stemness" genes using a bespoke epigenetics CRISPR library, we identify novel factors essential for transcription of key leukemia stem cell-associated oncogenes. We identify an important role for the SGF29 chromatin reader, and particularly its Tudor domain as a novel, attractive therapeutic target in AML.

INTRODUCTION

Acute Myeloid Leukemia (AML) is a devastating form of blood cancer with a dismal survival rate (1). Current therapies are often associated with strong toxicity and undesirable side effects, highlighting the need for safer, more effective alternatives. A major challenge in the development of new drugs for AML is the heterogeneity of the disease at the molecular level (2). AML is composed of several morphologic and molecular subtypes, with distinct mutational profiles and clinical characteristics (2).

However, there are molecular pathways that are commonly dysregulated across different AML subtypes. Studies have shown that a variety of upstream genetic alterations in AML, including DNMT3 mutations, NPM1 mutations and the gene fusion products of several different chromosomal translocations result in the activation of the clustered homeobox (HOX) genes and their co-factor proteins such as the three amino acid loop extension (TALE) homeobox gene MEIS1 (reviewed in (1–4)). Specific *HOX* genes such as the *HOXA* and/or *HOXB* genes as well as *MEIS1* display significantly higher expression in a large proportion of AML samples compared to normal bone marrow cells (3–6). In particular, highly elevated expression of posterior HOXA or B genes and *MEIS1* can be observed in as many as two-thirds of AML with diverse mutational profiles (7). Studies conducted using both loss-of-function as well as gain-of-function approaches have demonstrated the importance of *HOX/MEIS* expression in leukemia pathogenesis in diverse subsets of AML including those bearing MLL-fusions (5,6), NUP98-fusions (8), and AF10-fusions (9,10), to name a few. Importantly, ectopic *HOXA9* overexpression in murine hematopoietic stem and progenitor cells (HSPCs) causes a myeloproliferative phenotype in mice that can progress to AML upon *MEIS1*-co-expression (11,12). MEIS1 is a critical co-factor of leukemia-associated HOXA transcription factors and is required for their full leukemogenic capability (11,12). MEIS1 has also been shown to act as a rate-limiting regulator of leukemia stem cell (LSC) activity(13). Taken together, there is compelling evidence implicating the HOX/MEIS oncogenes as a key node integrating a variety of functionally distinct oncogenic insults in AML and possibly other leukemias.

These reports provide compelling preclinical evidence that pharmacological targeting of the HOX/MEIS pathway may yield therapeutic benefit in multiple, genetically heterogeneous AML sub-types. Since the HOX/MEIS proteins are DNA-binding transcription factors, they have proven difficult to target directly using traditional drug-development methods. We reasoned that a detailed and systematic identification of epigenetic modulators critical for sustaining HOX/MEIS-activation in AML would help identify novel nodes for targeted drug-discovery campaigns aimed at this clinically important pathway. To this end, we conducted pharmacological and CRISPR-based genetic screens using enhanced green fluorescence protein (eGFP) tagged MEIS1 cells (14). Our screens identified several novel regulators of HOX/MEIS expression in AML and

many of them were important for sustaining the expression of an array of leukemia oncogenes that drive AML including BMI1 and MYC. Most notably, our studies identified the Tudor domain-containing chromatin reader protein SGF29 as a critical epigenetic regulator required for maintaining transcription of key leukemia oncogenes and leukemogenesis of diverse AML subtypes.

RESULTS

A high-density, domain focused pooled CRISPR library screen identifies epigenetic regulators of *MEIS1* expression

AMLs with the t(10;11)(p13;q14) translocation - which results in the CALM-AF10 fusion gene - display elevated expression of several stem cell-associated factors including the HOXA cluster genes, MEIS1 and BMI1 (15,16). Indeed, AML cell lines with CALM-AF10 fusions display some of the highest expression of these oncogenes (Supplementary Fig. S1A). We used a CALM-AF10 positive AML cell line – U937 where the enhanced green fluorescence protein (eGFP) is knocked into the endogenous MEIS1 locus immediately upstream of the start codon (14). Leveraging this system, we sought to comprehensively identify epigenetic regulators of MEIS1 expression. First, we validated these U937-eGFP-MEIS1 cells (henceforth termed UB3) by perturbation with sgRNAs targeting DOT1L (Fig. 1A). Using these cells, we conducted a chemical compound screen using high-throughput flow-cytometry in a 384 well format assaying for eGFP levels (see Supplementary Fig. S1C for schematic). Screening with a library of 265 small-molecule compounds targeting epigenetic regulators (Supplementary Table S1) revealed only inhibitors of DOT1L and ENL, targets already established to regulate HOX/MEIS expression in AML (17–19) as “hits” - defined by >50% drop in eGFP-MEIS1 expression (Fig. 1B). Highly similar results were obtained in mouse MLL-AF9 transformed myeloid cells that we established from the bone marrow (BM) of a recently reported eGFP-MEIS1 transgenic mouse (Supplementary Fig. S1B). Since no novel MEIS1 regulators were identified in our small-molecule screens, we reasoned that this was likely due to limitations of the small-molecule library composition. A comprehensive collection of compounds targeting a wide variety of epigenetic regulators have not yet been developed and are therefore not

present in any of the commercially available epigenetic inhibitor libraries. Therefore, we sought to extend our investigation of MEIS1 epigenetic regulators using a genetic screening approach. Towards this end, we developed a high-density Epigenetics CRISPR (EpiC) library targeting 645 epigenetic regulators including chromatin readers, writers of histone acetylation, methylation and other modifications, genes involved in chromatin remodeling, transcription elongation, and DNA & RNA modifications in addition to control genes and non-targeting sgRNA controls (Supplementary Table S2). Studies have shown that targeting exons encoding functional domains may generate a higher proportion of null mutations and resulting in greater phenotypic selection compared to sgRNAs targeting early constitutive exons (20). Thus, we extracted the coding sequence corresponding to annotated protein domains available in Uniprot, for all our Epigenetics library genes (see Supplementary Methods). Then, we designed sgRNAs for the domain-encoding sequences on the Broad Institute Genetic Perturbation (GPP) Platform CRISPRko tool (21). We incorporated the 5 top-scoring sgRNAs of each annotated domain of every gene (see Methods). In addition to domain-focused sgRNAs, we designed 5 sgRNAs based on the standard early exon-targeting criterion. We used the EpiC library to conduct an in vitro phenotypic enrichment screen in single-cloned lentiviral Cas9-expressing UB3 cells. We hypothesized that dropouts in high- or low- eGFP fractions would help identify MEIS1 positive or negative regulators respectively. Thus, we FACS-sorted the top 25% and bottom 25% fractions based on eGFP levels (see Fig. 1D for schematic). Normalized read counts of non-targeting controls and polymerase-encoding genes were uniformly distributed in both high- and low- eGFP fractions, indicating the successful technical performance of controls (Supplementary Fig. S2A). Our analyses of the screen with the MAGeCKFlute (22,23) pipeline revealed several novel regulators, including AFF2, CSNK2A1, CSNK2B, SGF29/CCDC101, ENY2, TAF6, HDAC1 and LDB1, as well as most of the previously described epigenetic regulators of MEIS1 or HOX gene expression in AML, such as DOT1L (24–26), MLLT1/ENL (18,19), MLLT10/AF10 (24,27), KAT7/HBO1(28,29), JADE3 (28) and KMT2A/MLL1 (Fig. 1E). Analysis of the top candidate hits using the STRING database (17) showed that multiple proteins from six chromatin complexes were identified (Fig. 1F). This reinforced the possibility that we had identified distinct constituents of chromatin-modifying complexes

with MEIS1 regulatory activity – offering independent, complementary nodes for therapeutic targeting.

Competition assays reveal the role of MEIS1 regulators in AML cell growth

Next, we sought to test the requirement of our top candidate MEIS1 regulators for U937 cell growth. For this, we conducted arrayed CRISPR competition assays in UB3 cells (see Fig. 2A for schematic). Specifically, we cloned 2-3 sgRNAs for each of the top candidate hits (*SGF29, ENY2, AFF2, CSNK2A1, CSNK2B, MLLT1, KAT7,* and *JADE3),* in addition to DOT1L as a positive control, and non-targeting controls (NTC). For this, we used a plasmid vector co-expressing a blue fluorescence protein (BFP) and lentivirally transduced U937 cells at a ~50% transduction rate. We then sampled the populations by flow cytometry for up to 14 days and observed a significant ($P<0.05$, $n=3$) and progressive decline in the percentage of BFP positive cells targeted by all the candidate hits compared to NTCs over time (Fig. 2B). In addition, we observed a significant drop in eGFP fluorescence ($P<0.05$, $n=3$), for multiple sgRNAs targeting candidate hits, confirming a strong reduction in *MEIS1* expression (Supplementary Fig. S2B). In sum, these results indicate our phenotypic screening strategy uncovered high-confidence *MEIS1* regulators that affect the growth of U937 cells. In order to rule out that this anti-proliferative effect was limited to the CALM-AF10 positive cell line U937, we tested some of the novel MEIS1 regulators, including *CSNK2A1*, *ENY2,* and *SGF29* and controls in a Cas9-expressing MLL-AF9 fusion positive MOLM13 cell line (Supplementary Fig. S2C). CRISPR deletion of these genes also led to a progressive decline in the percentage of BFP positive cells compared to NTC-transduced cells, indicating that growth of MOLM13 cells also depended on these genes (Supplementary Fig. S2C). Interestingly, among these genes, the deletion of SGF29 and ENY2 had the most detrimental effects on the growth of both U937 as well as MOLM13-cells (Fig. 2B and Supplementary Fig. S2C).

CRISPR droplet-sequencing reveals leukemia oncotranscriptome targets of candidate regulators

Since we used MEIS1 as a surrogate reporter for the screen, we wanted to further evaluate the following: a) whether our candidate hits could regulate the expression not only of *MEIS1*, but also of other AML-associated oncogenes and b) which epigenetic regulators from our hits had the most pronounced effects on sustaining transcription of AML-promoting oncogenes. For this, we generated a targeted, small pooled CRISPR library containing 2-3 validated sgRNAs per candidate gene together with non-targeting controls (a total of 29 sgRNAs) and performed a single cell RNA-sequencing experiment in the UB3 cell line. Specifically, we used CRISPR droplet sequencing (CROP-Seq) (22), which allows for matching the single-cell RNA-sequencing profile of each cell to the sgRNA expressed within it, and thus infer knockout signatures of each of the CRISPR-deleted genes. After the assignment of sgRNAs to the pool of U937 cells, we performed unbiased clustering of whole transcriptome single cell RNA-seq data using the Ward.D2 minimum variance method (see Supplemental Methods) revealing the relatedness of each of the perturbations (Supplementary Figs. S2D and S2E). While the transcriptomes of CSNK2A1-, KMT2A- and MLLT10- knockout clustered together, DOT1L-, MLLT1-, AFF2- and SGF29- deleted transcriptomes formed a different cluster, indicating transcriptional similarities. Lastly, in our small pool, we also included sgRNAs for control genes which are either chromatin readers that do not show HOX/MEIS-specific gene regulatory activity in U937 cells (MLLT3, MLLT6), or have non-selective transcriptional effects (BRD4). Strikingly, analysis of the CROP-Seq data revealed that CRISPR deletion of several of the candidate epigenetic regulators, including AFF2, MLLT1, MLLT10, DOT1L, KAT7, SGF29, CSNK2A, and CSNK2B led to the downregulation not only of *MEIS1*, but also of several other leukemia and LSC-associated oncogenes (Fig. 2C and Supplementary Figs. S2G and S2F, and Supplementary Table S3). These downregulated genes included key genes of the *HOXA* cluster, *BMI1, SATB1*, *RNF220,* and *MSI2*. Moreover, their deletion also led to a concomitant increase in the expression of differentiation-associated genes such as lysozyme (LYZ), ELANE, the cathepsins CTSA and CTSD, and the S100A8/A9 proteins that are typically highly expressed in differentiated myeloid cells or involved in myeloid differentiation (Fig. 2D and Supplementary Fig. S2H). We then performed clustering of the single cell RNA-seq data using to investigate the transcriptomic relatedness of each perturbation to the others in

terms of their effects on *HOXA/MEIS* expression (see Supplemental Methods). Our analysis identified 3 major clusters. The first cluster comprises DOT1L, MLLT1, MLLT10, and AFF2. This cluster possibly reflects overlapping activities of these proteins that have been described to interact in multi-protein complexes (23–25). Interestingly, in our studies, AFF2, but not the super-elongation (SEC) complex constituent AFF4 was identified as a regulator of *HOX/MEIS1* expression in U937 cells (Fig. 1E, Fig. S2F and Supplementary Table S3). Similarly, the deletion of MLLT1, but not its homolog MLLT3, modulated *HOX/MEIS* expression in the UB3 cells, consistent with a prior study in a KMT2A-rearranged AML (8). Cluster 2 consisted of the genes KAT7, CSNK2A1, CSNK2B, and SGF29, whose deletion also had potent effects on the downregulation of *MEIS1* and other leukemia oncogenes (Fig. 2C, Fig. S2F and Supplementary Table S3). Cluster 3 consisted of the control genes we included in our CROP-Seq study, namely AFF4 and the chromatin readers BRD4 and MLLT3, whose deletion had no significant effects on *HOX/MEIS* or on differentiation-associated signatures in the setting of the UB3 cell line. Taken together, our studies showed that several epigenetic regulators identified in our eGFP-MEIS1 screen were important for sustaining key LSC signature genes and in reversing the differentiation block in U937 cells.

CRISPR dependency assays earmark SGF29 as an AML-selective dependency

One of the challenges in developing epigenetic candidates as therapeutic candidates is that drugging some of these candidates has the potential for non-selective toxicity. One way of assessing the selectivity of a candidate gene as a therapeutic target is to investigate the effect of its genetic depletion in the cancer dependency maps (DepMap) dataset, a database of genome-scale functional genetic screens in hundreds of cancer cell lines (26). We assessed our top candidate epigenetic regulators for efficacy (the degree to which CRISPR knockout of the candidate gene reduces cell fitness in sensitive lines), and selectivity (the degree of differences in its essentiality across all cancer cell lines) using the Shiny DepMap application which combines CRISPR and shRNA data from diverse cancer cell lines (27). Our analyses showed that some of the novel candidate hits identified in our screen, including SGF29, ENY2 and CSNK2A1, as well as previously

characterized genes such as DOT1L, MLLT1, MLLT10 and KAT7 had a higher selectivity compared to pan-essential genes such as PSMA4 or even the chromatin reader BRD4 (Fig. S2I). Next, since several of our candidate epigenetic regulators seemed to regulate the expression of AML-promoting oncogenes, we wanted to assess whether depletion of any of our candidate hits would selectively affect the fitness of AML cell lines compared to cancer cell lines derived from other lineages. For this, we assessed the differences in median CRISPR knockout fitness scores (Chronos) between 26 AML cell lines in the AML DepMap data and 1,060 non-AML cancer cell lines. This analysis showed that while some of the hits identified in our screen were highly AML selective, others were not. Specifically, the most AML-selective genes from our candidate hits were MLLT1, SGF29, DOT1L, AFF2 and KMT2A (ranked in decreasing order of AML selectivity as assessed by Wilcox test of AML Vs Non-AML cell line dependency scores) (Fig. 2D). Other chromatin regulators, namely MLLT10, CSNK2A1/2, CSNK2B, JADE3 and ENY2 were not AML selective (FDR p value <0.05). In other words, depletion of the AML-selective hits significantly impaired the fitness of AML compared to non-AML cell lines. This data provides an indication that the AML-selective candidate genes may serve as more selective therapeutic targets in terms of designing anti-AML therapies. Of particular interest was SGF29, in terms of novelty, effect on leukemogenic gene expression programs and high AML selectivity across 1,086 cancer cell types (Fig. 2E and 2F).

SGF29 deletion has pronounced anti-leukemia effects in cell-line-derived and patient-derived AML models

Since our transcriptomic, single sgRNA validation, and computational studies showed that SGF29 was one of the strongest dependencies from our hits across AML cell lines, we sought to directly assess the impact of *SGF29* deletion on human AML cell growth and leukemogenesis. Consistent with our flow cytometry-based *in vitro* competition assays (Fig. 2B and Supplementary Fig. S2C), we observed that SGF29 inactivation using validated CRISPR sgRNAs (Supplementary Fig. S3A) led to significantly increased retention of the dye Cell Trace Violet (see Methods) in both U937 as well as MOLM13 AML cell lines, indicating diminished proliferation compared to cells treated with non-

targeting controls (Figs. 3A and 3B). Furthermore, the antiproliferative effects of SGF29 deletion were accompanied by a significant increase in the proportion of cells in the G0/G1 fraction compared to SGF29 wild-type cells (Supplementary Fig.S3B). SGF29 deleted cells also showed a striking and significantly increased uptake of fluorescence -labeled heat-inactivated *E coli* bioparticles, indicating that SGF29 inactivation led to the myeloid differentiation of U937 cells (Fig. 3C and 3D). Next, we performed bulk RNA sequencing of MOLM13 and U937 cells with SGF29 CRISPR knockout compared to non-targeting control (NTC) cells. Our RNA-seq analysis showed that SGF29 deletion significantly decreased the expression of several *HOXA* cluster genes in addition to *MEIS1* in both MOLM13 and U937 cells (Figs. 3E & 3G), confirming its role in *HOX/MEIS* regulation in diverse AML subtypes. Further, there was also a significant reduction in the expression of MYC (Fig. S3C) and the expression of MYC target genes was strikingly enriched in the non-targeting control AML cells compared to the SGF29 deleted counterparts, as assessed using gene-set enrichment analysis (GSEA) (28) (Fig.S3D). Given these strong effects of SGF29 deletion on leukemia oncogene expression and on AML cell growth, we then tested whether SGF29 deletion affected *in vivo* leukemogenesis of these human AML cell lines. We performed *in vivo* studies using a cell line-derived xenograft model of leukemogenesis in NOD.Cg-*Rag1*^{tm1Mom} *Il2rg*^{tm1Wjl}/SzJ (NRG) mice, showed that SGF29 deletion led to a significantly increased disease latency in Cas9-expressing U937 as well as MOLM13 cell lines (Fig. 3F).

Genetic Sgf29 inactivation impairs the clonogenicity of transformed but not normal hematopoietic progenitors

Next, given the role of SGF29 in influencing the transcription of self-renewal-associated genes, we wanted to test the effect of *Sgf29* depletion on the clonogenic capability of myeloid bone marrow (BM) cells transformed by distinct AML driver oncoproteins. We therefore performed methylcellulose-based colony forming unit (CFU) assays on murine bone marrow hematopoietic stem and progenitor cells (HSPCs) transformed using the CALM-AF10, MLL-AF10 or MLL-AF9 oncofusion proteins. Our studies showed that CRISPR knockout using two validated, (Supplementary Fig. S4A) retrovirally expressed

sgRNAs targeting *Sgf29* coding exons led to a significant reduction in the number of colonies with a blast-like morphology in BM cells transformed with CALM-AF10 fusion oncoprotein, compared to the corresponding cells with an sgRNA targeting the *Sgf29* intronic region (Fig. 4A-C). Interestingly, while there was a dramatic decrease in the numbers of immature blast-like colonies, there were relatively modest effects on the number of differentiated colonies; thus, most colonies in the Sgf29 -/- arm bore a differentiated morphology (Fig. 4B). The strong reduction in blast colony formation persisted for at least two rounds of replating (Supplementary Fig. S.4B.). At the cellular level, in contrast to the immature, myeloid blast-like cellular morphology observed in Wright-Giemsa-stained cytospins of cells with wild-type *Sgf29*, the *Sgf29* knockout cells resembled terminally differentiated, or differentiating myeloid lineage cells (Fig. 4C). Similar results were obtained from BM cells transformed using MLL-AF9 (Fig. 4D-F) and MLL-AF10 (Fig. 4G-I) fusion oncoproteins. *Sgf29* deleted cells also showed increased apoptosis compared to *Sgf29* wild-type cells as measured by immunoblotting for cleaved PARP (Supplementary Fig. S4E). Next, we wanted to test the effect of Sgf29 deletion on the colony forming ability of normal HSPCs using the same sgRNAs that showed striking reductions in the formation of immature, blast-like colonies in myeloid transformed cells. Interestingly, in contrast to BM cells transformed using AML oncoproteins, CRISPR-mediated Sgf29 deletion in murine lineage negative, Sca-1 positive, Kit-positive (LSK) cells did not significantly alter either the number or type of colonies observed in CFU assays (Fig. 4J-K). Taken together, these data indicate that *Sgf29* inactivation influences the clonogenicity and differentiation of cells transformed by diverse AML oncoproteins, but not normal hematopoietic stem and progenitor cells (HSPCs).

The Tudor domain of SGF29 is essential for its role in myeloid transformation

The SGF29 protein harbors a carboxy (C)-terminal tandem Tudor domain and this region is important in recognition of H3K4 di/trimethylated chromatin modifications and recruitment of KAT2A (GCN5)-containing chromatin-modifying complexes (29–31). In our epigenetic CRISPR screen, we identified that top-performing sgRNAs for SGF29 had homology to its Tudor domain, which confers H3K4me2/3 reader activity to SGF9. Thus,

we hypothesized that this domain may be required for the transcriptional activation of AML oncogenes including the HOX/MEIS genes, BMI1 and MYC. To assess the dependency of the Tudor domain for SGF29 localization in the HOX/MEIS loci, we cloned a Flag-tagged SGF29 gene and generated a stably transduced U937 cell line. Similarly, in order to test the effect of the SGF29 Tudor domain we also generated U937 cells expressing the SGF29^{D196R} mutant, which has been shown to disrupt H3K4me3 binding. (29). ChIP-sequencing using a Flag antibody in the Flag-SGF29 U937 cells showed that the protein occupied regions that were enriched for H3K4me3 marked active promoters and H3K27 acetylated enhancers (Fig. 5A&B). SGF29 occupied the promoter and/or enhancer regions of HOX/MEIS genes as well as other AML oncogenes whose expression was dependent on SGF29 (including BMI1 and MYC) (Fig. 5C). Interestingly, our analysis showed that in contrast to the wildtype SGF29, binding of the SGF29^{D196R} mutant to these gene loci was almost obliterated in SGF29^{D196R} mutant-expressing U937 cells (Fig. 5C). Next, we wanted to assess whether the Tudor domain was important for the clonogenic capability of leukemia cells using the CFU assay. For this, we used the mouse MLL-AF9-transformed bone marrow cells which lose blast-like colony formation upon endogenous Sgf29 deletion. Using these cells, we reinstated wither wildtype human SGF29 (impervious to the mouse anti-Sgf29 sgRNAs) or the SGF29^{D196R} mutant counterpart using retroviral overexpression (Fig. 5D). Interestingly, CFU assays demonstrated that ectopic overexpression of wildtype, but not mutant SGF29 could completely rescue the loss of blast-like CFUs upon endogenous *Sgf29* deletion (Fig. 5D). Notably, ectopic expression of the SGF29^{D196R} mutant itself dramatically reduced the number of blast-like colonies even in MLL-AF9 cells with intact endogenous Sgf29 alleles, indicating that the SGF29^{D196R} mutant has dominant negative activity in the MLL-AF9 transformed cells (Fig. 5D).

Chromatin proteomics reveal the role of SGF29 in chromatin localization of proteins with established roles in AML pathogenesis

We sought to identify the molecular mechanism by which SGF29 elicits its effects on the transcription of leukemia oncogenes. SGF29 is a participant of distinct chromatin

regulatory complexes including the ADA2A-containing (ATAC) complex and the SPT3-TAF9-GCN5-acetyltransferase complex (STAGA) complex; the mammalian homolog of the yeast SAGA (SPT-ADA-GCN5-acetyltransferase complex). Both these complexes harbor the KAT2A (GCN5) and KAT2B (PCAF) acetyltransferases with histone acetylating activity and prominent roles in transcriptional activation(32). Thus, we sought to investigate which epigenetic regulators are evicted from chromatin upon SGF29 depletion in AML cells. For this, we performed chromatin enrichment proteomics (ChEP) (33) (see Fig. 6A for schematic). This method allows an unbiased quantitative and qualitative assessment of the chromatin-associated proteome (33). Our ChEP purification yielded substantial enrichment of the chromatin/nuclear fraction as measured by the high proportional abundance of histones, histone modifying proteins, transcription factors and other chromatin and nuclear-associated proteins in the enriched fractions (Fig. 6B and Supplementary Fig. S5A). *SGF29* deletion in U937 cells significantly decreased the abundance of key AML oncoproteins, as measured by the intensity of chromatin-associated peptides by mass spectrometry. Specifically, the levels of HOXA13 and SATB1 were were significantly reduced in the chromatin fraction of SGF29 deleted cells in contrast to their wildtype counterparts and the levels of MEIS1 and MYC were essentially undetectable in the chromatin fraction of SGF29 deleted cells in contrast to their SGF29 wildtype counterparts, where these proteins were highly abundant. (Figs. 6C-D and Supplementary Fig. S5B). We also observed a significant decrease in the abundance of CDK4 and CDK6 proteins, involved in cell cycle regulation and known to play prominent roles in the proliferation of cancer cells, particularly in AML (34). Most importantly, our ChEP data analysis demonstrated that SGF29 deletion led to a significant decrease in the chromatin abundance of key components of the STAGA complex, the histone acetyltransferase KAT2A, as well as the transcriptional adaptor protein TADA3 (Fig. 6C and Supplementary Fig. S5B). These striking results indicate that SGF29 deletion may lead to eviction of the STAGA complex from the chromatin fraction of U937 cells. In order to test this using an orthogonal approach, we performed dot blots by immunoblotting using a KAT2A specific antibody in different cellular fractions in the SGF29 wildtype or CRISPR-deleted AML cells. Our studies demonstrated that while KAT2A could be found mostly in the chromatin fraction in wildtype U937 cells, SGF29

deletion indeed led to an increased abundance of KAT2A in the cytoplasmic fraction (Fig. 6E).

SGF29 deletion diminishes H3K9Ac on the promoters of key leukemia oncogenes

Our results showing that SGF29 deletion decreased the abundance of the histone acetyltransferase KAT2A in the chromatin fraction led us to hypothesize that SGF29 is important for recruiting the chromatin activity of KAT2A on AML oncogene loci. KAT2A is the acetyltransferase subunit of the SAGA complex that plays important roles in leukemia and other cancers and is being currently pursued as a promising therapeutic target for drug development. To test whether SGF29 affects the activity of KAT2A on chromatin, we performed ChIP-seq for H3K9Ac, the major histone modification deposited by the SAGA complex that is associated with transcriptional activation (32). Our analysis of the ChIP-seq data showed that upon SGF29 deletion, there were striking changes in H3K9 acetylation, with 10,834 peaks showing reduced acetylation and 3,119 peaks showing increased acetylation in SGF29 knockout compared to wildtype U937 cells (Fig. 7A, and Supplementary Fig. S6A). Importantly, there was a pronounced decrease in acetylation levels at the promoter of several AML oncogenes that were also transcriptionally downregulated in the SGF29 knockout RNA-seq data. This included *HOXA* cluster genes, MYC, BMI1, and SATB1 – all *bona fide* AML oncogenes with established roles in augmenting leukemic self-renewal (Fig. 7B).

SGF29 deletion impairs *in vitro* and *in vivo* leukemogenesis in a patient-derived xenograft model of AML

We then wanted to assess the effect of SGF29 deletion in a human AML patient cells. For this, we used AML393 cells, derived from an AML patient; these cells express split-Cas9 and can be used to perform gene-editing in a human AML sample (35). In AML393 cells, SGF29 knockout using the BFP-co-expressing sgRNAs led to a striking reduction in proliferative advantage in a competition assay compared to non SGF29-sgRNA expressing cells (Fig. 7C) and quantitative real-time PCR (q-RT-PCR) of SGF29-knockout compared to non-targeting control transduced AML393 cells showed a significant reduction of *HOXA9* and *MEIS1* transcripts in SGF29 deleted cells (Fig. 7D). We then

injected the AML393 cells with SGF29 knockout or non-targeting controls (NTC) into NRG mice and monitored engraftment of human CD45+ cells by flow-cytometric assessment of peripheral blood. Strikingly, in comparison to the AML CDX models described in Fig. 3F&H, we observed much more pronounced effects of SGF29 deletion in this human PDX model of AML. Whereas mice injected with NTC-targeting sgRNAs succumbed to AML with a median latency of 64 days, those injected with sgRNAs targeting SGF29 showed had a median disease latency of 165 days post injection (Fig. 7E).

Taken together, our results demonstrate that SGF29 is important for sustaining critical transcriptional networks in leukemogenesis and may serve as an attractive therapeutic target in AML.

DISCUSSION

SGF29 was discovered in yeast as a component of the SAGA (Spt–Ada–Gcn5 acetyltransferase) complex (36). Later studies showed that Sgf29 is highly conserved across several species and is also an important constituent of the STAGA complex (the mammalian homolog of the SAGA complex) (Reviewed in (37,38). SGF29 was shown to have two tandem Tudor domains at the C-terminus that were discovered to specifically bind to H3K4 di and trimethylation (29,30). The chromatin reading activity of the SGF29 Tudor domains is important for the recruitment of the SAGA complex to chromatin and consequently for histone acetylation and transcriptional activation of target genes. In human cells, SGF29 was shown to regulate MYC expression in hepatocellular carcinoma (39). We observe that SGF29 is an important regulator of the transcription as well as chromatin abundance of several leukemia-associated transcription factors in AML cells and plays an important role in sustaining the leukemogenesis of diverse AML oncoproteins.

FIGURE LEGENDS:

Figure 1 Screening for epigenetic modulators identifies novel MEIS1 regulators in AML cells **(A)** GFP-MEIS1 signal in U937 GFP-MEIS1 AML upon DOT1L CRISPR knockout is plotted on the y-axis. Biological duplicates indicate independent sgRNAs. The y axis indicates eGFP intensity. (B) Small-molecule screen in human U937 GFP-MEIS1 AML cells; y-axis indicates the percentage GFP-Meis1 intensity compared to controls on day 5 of treatment with the small molecule library; x-axis indicates a compound number assigned to list the compounds in the library. (C) Bubble plot to illustrate the categories of chromatin modulators included in the library design; the numbers indicate the different genes under the category and the size of the bubble is proportional to the gene-set size. Controls refer to pan-essential genes. (D) Strategy for phenotypic pooled CRISPR screening of epigenetic regulators for MEIS1 expression in the U937 cell line with an eGFP-MEIS1 endogenous knock in tag. (E) Sorted gene hits based on differential beta scores for the eGFP-MEIS1 low minus eGFP-MEIS1 high fractions. Beta scores were calculated using MAGeCKFlute. (F) Annotated protein complexes comprising top candidate hits identified in the epigenetic screen as identified using String database analysis are shown. Hits from the Epigenetics CRISPR library screen are marked with a glowing hue within the protein complex.

Figure 2. Requirement for MEIS1 regulators for transcriptomic changes and AML cell growth: (A) Schematic of competition assay with cells transduced with sgRNAs expressed in a BFP+ backbone. The proportion of BFP positive cells is assessed over time using flow-cytometry. (B) The y-axis indicates flow cytometry measurements of the percentage of U937 BFP+ cells over time, normalized to the baseline (time 0 or T”0”) measurement; the x-axis indicates the sgRNA number for non-targeting controls (NTC) or each gene (n=2). Each bar represents a timepoint measurement: baseline, day 8, day 11, and day 14. (C) Ridge plots for CROP-Seq perturbations. Knockout genes are indicated on the y-axis and RNA expression levels for the (A) self-renewal associated or (B) differentiation-associated genes listed are on the x-axis. The median expression value is indicated. (E) A relative score of DepMap dependencies for AML (n=26) compared to non-AML cell lines (n=1080) is shown for candidate hits identified in our screen. Y-axis is rank of AML selectivity, and x-axis shows the negative log 10 p-value. (F) A sigmoid plot of DepMap

data showing the dependency score (Chronos – x-axis), compared to the normalized dependency rank (y-axis) for SFG29 in 1,086 cancer cell lines.

Figure 3. Proliferative and transcriptional effects of SGF29 loss in AML. (A) Retention of the CellTrace™ Far Red dye in **(A)** U937 or **(B)** MOLM13 cells transduced with an SGF229 sgRNA (top) compared to non-targeting control (NTC), measured by flow cytometry over time. **(C)** Schematic for differentiation assessment via phagocytosis of fluorescently labeled E. coli bioparticles. **(D)** Histograms of U937 cells transduced with an NTC (grey) or an SGF29 sgRNA (violet) show the fluorescence intensity of engulfed pHrodo™ Red E. coli bioparticles measured at 9 days after staining. Effect of SGF29 deletion on the transcription of HOXA/MEIS genes in **(E)** U937 or **(G)** MOLM13 AML cell lines, compared to non-targeting control (NTC) is shown. TPM: transcripts per million, P val. *<0.05, **<0.01, ***<0.005. (F) Kaplan-Meier curves for NTC versus SGF29 knockout in **(F)** U937 and **(H)** MOLM13 AML cell lines and an MLL-AF10 patient-derived xenograft line.

Fig.4. *Sgf29* deletion impairs the clonogenicity of transformed but not normal hematopoietic cells: A) Number of colony-forming units (CFU) from CALM-AF10 transformed cells transduced with Sgf29 intron-targeting sgRNA (Sgf29-Int) or two independent Sgf29 exon-targeting sgRNAs are shown. CFUs per 2,000 plated cells at 1 week are plotted on the Y-axis, and colonies are divided into those with a blast-like or a differentiated colony morphology. **B)** Pictures of representative colonies with each of the labelled sgRNA-transduced cells are shown. Scale bar: 100 mm. **C)** Wright-Giemsa-stained cytospins of representative cells from each of the CRISPR perturbations are shown. Scale bar: 10 mm. The same experiments as shown for CALM-AF10 transformed BM cells shown in (**A-C)** are shown for MLL-AF9-transformed BM cells in (**D-F**) and MLL-AF10-transformed cells in (**G-I**). **J**) CFUs per 10,000 lineage negative, Sca-1 positive, Kit positive (LSK) cells with Sgf29 deletion (Sgf_sg1) compared to Sgf29 wildtype LSKs (non-targeting control; NTC) are shown. Y-axis shows the numbers of different types of

colonies, with each plot indicating a separate kind of morphologically distinct CFU in this assay. P values: *= p<0.05, ** = P<0.01.

Figure 5. Evaluation of the Tudor domain of SGF29 activity in AML cells

(A) Proportion of SGF29 peaks in promoter regions and intergenic regions in U937 cells are shown in the Donut plot.

(B) SGF29 peaks in promoter regions and their associated with H3K4me3, and intergenic, intronic and other regions marked by H3K27ac in U937 cells are shown in the bar graph as marked. X-axis shows number of peaks.

(C) Genome tracks depicting normalized reads (y-axis) for wildtype or mutant SGF29 at the genomic locus of the HOXA/MEIS1, MYC, and BMI1 genes in U937 cells are shown. **(D)** Top panel: Representative images of CFUs from MLL-AF9 transformed bone marrow cells with a mock transduction (two top left colonies), non-targeting control (two top middle colonies) or Sgf29 sgRNA (two right colonies) are shown. Middle panel: Same cells as above, but with ectopic retroviral overexpression of wildtype human SGF29 impervious to SGF29 sgRNA. Lower panel: Same MLL-AF9 transformed cells as in top panel but with retroviral overexpression of the human SGF29D196R mutant is shown. Representative colonies are shown in bright field at 20x magnification.

Figure 6. Chromatin enrichment proteomics reveals SGF29-dependent proteins in the chromatin proteome **(A)** Schematic for the ChEP sample preparation, as previously described (33) . **(B)** A donut plot showing the functional protein categories in proteomic analysis of the ChEP SGF29-deleted fraction across 4 samples. Proteins were annotated using the categories outlined in (33). The number of proteins per category is shown in parentheses. **(C)**Volcano plots depicting -log(10) of the adjusted P value on the y-axis and log(2) of fold change (LogFC) of all proteins in the ChEP fractions for both SGF29 knockout vs. NTC. Differentially abundant protein (Absolute FC >2, Adj. P value. < 0.05 are not shown; n=3 for every experimental condition. **(D)** Bar graphs depicting intensity values for self-renewal-associated proteins enriched by ChEP in the SGF29 knockout vs

NTC experiment. **(E)** Dot blots for ChEP-enriched chromatin, cytoplasmic fraction, and whole-cell lysate for NTC and SGF29 knockout are shown. Vinculin and Histone H3 were included as cytoplasmic and chromatin protein controls respectively.

Figure 7. Effect on H3K9 acetylation and antileukemia activity of SGF29 in AML patient cells **(A)** Volcano plot indicating changes in H3K9 acetylation across the genome in UB3 cells after deletion of SGF29. Blue dots are the loci with decreased and red are the loci with increased acetylation. **(B)** Integrated genome viewer (IGV) tracks showing ChIP-seq peaks for H3K9ac on AML oncogene loci in U937 cells expressing non-targeting (grey), compared to SGF29 targeting sgRNAs (blue). **(C)** *In vitro* competition assay is shown with percentage of SGF29 sgRNA expressing BFP positive AML393 human AML cells (y-axis) is shown in blue bars, compared to control cells in grey. Progressive percentage of BFP is shown over time at indicated timepoints shown on the y-axis. **(D)** Relative expression of *HOXA9* and *MEIS1* in SGF29 deleted AML393 cells is plotted on the y-axis normalized to the SGF29 wildtype control (n=3). P values: **= $p<0.05$, *** = $P<0.01$. **(E)** Kaplan-Meier curves for NTC versus SGF29 deleted AML393 PDX (MLL-AF10 positive) are shown with the survival probability plotted on the y-axis.

METHODS:

Animal Studies

All animal studies were approved and performed as per the guidelines of SBP Medical Discovery Institutional Animal Care and Use Committee. 200 uL of 200,000 UB3 or MOLM13 cells expressing Cas9 and NTC or SGF29 targeting sgRNA were injected intravenously by tail vein injections into NOD/SCID mice (SBP Animal Resources). Mice were monitored every day and sacrificed when critically ill. For MLL-AF10 PDX studies, 150,000 cells expressing split Cas9 and NTC or SGF29 sgRNA were injected into NSG mice (Jackson Laboratories) by tail vein injections. Mice were bled at every 2 to 3 weeks for checking AML cell engraftment by flow cytometry. Animals were sacrificed when critically ill.

Cell culture

Human leukemia cell lines U937 (kind gift from Dr. Daniel Tenen, Beth Israel Deaconess Medical Center) and MOLM13 (ACC-554, DSMZ), were cultured in RPMI-1640 medium supplemented with 2 mM L-glutamine and sodium pyruvate, 10% Fetal bovine serum and 50 U/ml Penicillin/Streptomycin (Thermo Fisher Scientific, Carlsbad, CA), 2 mM L-glutamine and incubated in 5% CO2 at 37°C. Murine leukemia cells were cultured in DMEM medium supplemented with 2 mM L-glutamine, 15% FBS and 50U/ml Penicillin/Streptomycin, in the presence of following cytokines: 10 ng/ml murine interleukin 6 (mIL-6), 6 ng/ml murine interleukin 3 (mIL3) and 20 ng/ml murine stem cell factor (mSCF) (all from Peprotech, Rocky Hill, NJ), and incubated at 5% CO2 and 37°C. HEK293T cells were cultured in DMEM medium supplemented with 2 mM L-glutamine and sodium pyruvate, 10% FBS and 50 U/ml Penicillin/Streptomycin, and incubated in 5% CO2 at 37°C. MLL-AF10 patient derived xenograft (PDX) cells were cultured in IMDM medium supplemented with 20% BIT9500 (STEMCELL Technologies), human cytokines and StemRegenin 1 44 (SR1) and UM171 as described earlier(40).

CRISPR Screen data analysis

Fastq files from the epigenetics CRISPR screen were analyzed using the MAGeCK-VISPR MLE pipeline (41). Gene-rankings were generated comparing the GFP -low and -high fractions to T0. Both experimental conditions were further compared using MAGeCKFlute (42). For subsequent functional hit-validation, the 15 genes with the greatest differences in beta scores in the GFP-Low minus GFP-High conditions were considered as candidate epigenetic regulator hits.

Data availability

Sequencing data for RNA-seq, ChIP-seq, high-throughput CRISPR screens, and CROP-seq are deposited the NCBI GEO under accession number: GSE217829. The sgRNA sequences used for the Human Epigenetic Library is deposited in: https://github.com/kobarbosa/HOX-Manuscript.

Authors contributions

K.B. and **A.D**. contributed equally to the study. **KB.:** conceptualization, data curation, formal analysis, funding acquisition, investigation, methodology, project administration, software, supervision, validation, visualization, writing-original draft. **A.D.:** conceptualization, data curation, formal analysis, investigation, methodology, project administration, software, supervision, validation, visualization, writing-original draft. **M.P.:** investigation, visualization, validation**. P.X.:** resources. **R.K.H.:** resources. **R.M**: data curation, formal analysis, methodology, software*.* **A.M.:** data curation, formal analysis, methodology, software. **N.R.:** data curation, formal analysis, methodology, software. **F.S.:** data curation, formal analysis, methodology, software. **X.L.:** data curation, formal analysis, software**. Y.S.:** investigation. **A.B.:** resources, software. **J.D.:** resources, software. **P.M.:** resources**. E.R.:** conceptualization, resources, software. **J.S.:** conceptualization, resources. **P.D.A.:** conceptualization, resources. **A.J.D.:** conceptualization, resources, funding acquisition, investigation, methodology, project administration, supervision, visualization, writing-original draft.

Acknowledgements

The authors gratefully acknowledge Dr. Irmela Jeremias for providing the MLL-AF10 positive AML393-Cas9 cells. We would like to thank Adriana Charbono and Buddy Charbono for their invaluable assistance with mouse studies. Dr. Chih-Cheng Yang and Dr. Chun-Teng Huang from the Sanford Burnham Prebys Medical Discovery Institute (SBP) functional genomics core, Yoav Altman from the SBP Flow Cytometry Core, and Dr. Kang Liu from the Genomics Core for their excellent support. We would like to acknowledge help from Dr. Philip Koeffler, Dr. Gery Sigal, Dr. Sarah Parker and Dr. Aleks Scotland for their help with chromatin proteomics at Cedars Sinai.

This work was supported by National Institutes of Health (NIH) National Cancer Institute grants CA262746 and P30 CA030199, the Rally Foundation for Childhood Cancer Research and the Luke Tatsu Johnson Foundation grant (Award number 22IC33), an Emerging Scientist Award from the Children's Cancer Research Fund (Award Number

20IC17), and the V Foundation for Cancer Research (TVF) under award number DVP2019-015.

REFERENCES

1. Dohner H, Weisdorf DJ, Bloomfield CD. Acute Myeloid Leukemia. N Engl J Med. 2015;373:1136–52.

2. Papaemmanuil E, Döhner H, Campbell PJ. Genomic classification in acute myeloid leukemia. N. Engl. J. Med. 2016. page 900–1.

3. Abramovich C, Pineault N, Ohta H, Humphries RK. Hox genes: from leukemia to hematopoietic stem cell expansion. Ann N Y Acad Sci. Wiley; 2005;1044:109–16.

4. Argiropoulos B, Humphries RK. Hox genes in hematopoiesis and leukemogenesis. Oncogene. 2007;26:6766–76.

5. Alharbi RA, Pettengell R, Pandha HS, Morgan R. The role of HOX genes in normal hematopoiesis and acute leukemia. Leukemia. 2013;27:1000–8.

6. Collins CT, Hess JL. Deregulation of the HOXA9/MEIS1 axis in acute leukemia. Curr Opin Hematol. 2016;23:354–61.

7. Spencer DH, Young MA, Lamprecht TL, Helton NM, Fulton R, O'Laughlin M, et al. Epigenomic analysis of the HOX gene loci reveals mechanisms that may control canonical expression patterns in AML and normal hematopoietic cells. Leukemia. Springer Science and Business Media LLC; 2015;29:1279–89.

8. Wang GG, Cai L, Pasillas MP, Kamps MP. NUP98-NSD1 links H3K36 methylation to Hox-A gene activation and leukaemogenesis. Nat Cell Biol. Springer Science and Business Media LLC; 2007;9:804–12.

9. Caudell D, Zhang Z, Chung YJ, Aplan PD. Expression of a CALM-AF10 fusion gene leads to Hoxa cluster overexpression and acute leukemia in transgenic mice. Cancer Res. 2007;67:8022–31.

10. DiMartino JF, Ayton PM, Chen EH, Naftzger CC, Young BD, Cleary ML. The AF10 leucine zipper is required for leukemic transformation of myeloid progenitors by MLL-AF10. Blood. American Society of Hematology; 2002;99:3780–5.

11. Thorsteinsdottir U, Mamo A, Kroon E, Jerome L, Bijl J, Lawrence HJ, et al. Overexpression of the myeloid leukemia-associated Hoxa9 gene in bone marrow cells induces stem cell expansion. Blood. American Society of Hematology; 2002;99:121–9.

12. Kroon E, Krosl J, Thorsteinsdottir U, Baban S, Buchberg AM, Sauvageau G. Hoxa9 transforms primary bone marrow cells through specific collaboration with Meis1a but not Pbx1b. EMBO J. Wiley; 1998;17:3714–25.

13. Wong P, Iwasaki M, Somervaille TC, So CW, Cleary ML. Meis1 is an essential and rate-limiting regulator of MLL leukemia stem cell potential. Genes Dev. 2007;21:2762–74.

14. Xiang P, Yang X, Escano L, Dhillon I, Schneider E, Clemans-Gibbon J, et al. Elucidating the importance and regulation of key enhancers for human MEIS1 expression. Leukemia [Internet]. 2022; Available from: http://dx.doi.org/10.1038/s41375-022-01602-4

15. Barbosa K, Deshpande A, Chen B-R, Ghosh A, Sun Y, Dutta S, et al. Acute myeloid leukemia driven by the CALM-AF10 fusion gene is dependent on BMI1. Exp Hematol. 2019;74:42-51 e3.

16. The role of CALM-AF10 gene fusion in acute leukemia [Internet]. Leukemia 2008 page 678–85. Available from: http://dx.doi.org/10.1038/sj.leu.2405074

17. Daigle SR, Olhava EJ, Therkelsen CA, Majer CR, Sneeringer CJ, Song J, et al. Selective killing of mixed lineage leukemia cells by a potent small-molecule DOT1L inhibitor. Cancer Cell. 2011;20:53–65.

18. Erb MA, Scott TG, Li BE, Xie H, Paulk J, Seo HS, et al. Transcription control by the ENL YEATS domain in acute leukaemia. Nature. 2017;543:270–4.

19. Wan L, Wen H, Li Y, Lyu J, Xi Y, Hoshii T, et al. ENL links histone acetylation to oncogenic gene expression in acute myeloid leukaemia. Nature. 2017;543:265–9.

20. Shi J, Wang E, Milazzo JP, Wang Z, Kinney JB, Vakoc CR. Discovery of cancer drug targets by CRISPR-Cas9 screening of protein domains. Nat Biotechnol. 2015;33:661–7.

21. Doench JG, Fusi N, Sullender M, Hegde M, Vaimberg EW, Donovan KF, et al. Optimized sgRNA design to maximize activity and minimize off-target effects of CRISPR-Cas9. Nat Biotechnol. Springer Science and Business Media LLC; 2016;34:184–91.

22. Datlinger P, Rendeiro AF, Schmidl C, Krausgruber T, Traxler P, Klughammer J, et al. Pooled CRISPR screening with single-cell transcriptome readout. Nat Methods. 2017;14:297–301.

23. Okada Y, Feng Q, Lin Y, Jiang Q, Li Y, Coffield VM, et al. hDOT1L links histone methylation to leukemogenesis. Cell. 2005;121:167–78.

24. Mueller D, Bach C, Zeisig D, Garcia-Cuellar MP, Monroe S, Sreekumar A, et al. A role for the MLL fusion partner ENL in transcriptional elongation and chromatin modification. Blood. 2007;110:4445–54.

25. Luo Z, Lin C, Guest E, Garrett AS, Mohaghegh N, Swanson S, et al. The super elongation complex family of RNA polymerase II elongation factors: gene target specificity and transcriptional output. Mol Cell Biol. 2012;32:2608–17.

26. Tsherniak A, Vazquez F, Montgomery PG, Weir BA, Kryukov G, Cowley GS, et al. Defining a Cancer Dependency Map. Cell. 2017;170:564-576 e16.

27. Shimada K, Bachman JA, Muhlich JL, Mitchison TJ. shinyDepMap, a tool to identify targetable cancer genes and their functional connections from Cancer Dependency Map data. Elife [Internet]. eLife Sciences Publications, Ltd; 2021;10. Available from: http://dx.doi.org/10.7554/eLife.57116

28. Subramanian A, Tamayo P, Mootha VK, Mukherjee S, Ebert BL, Gillette MA, et al. Gene set enrichment analysis: a knowledge-based approach for interpreting genome-wide expression profiles. Proc Natl Acad Sci U S A. 2005;102:15545–50.

29. Bian C, Xu C, Ruan J, Lee KK, Burke TL, Tempel W, et al. Sgf29 binds histone H3K4me2/3 and is required for SAGA complex recruitment and histone H3 acetylation. EMBO J. Wiley; 2011;30:2829–42.

30. Vermeulen M, Eberl HC, Matarese F, Marks H, Denissov S, Butter F, et al. Quantitative interaction proteomics and genome-wide profiling of epigenetic histone marks and their readers. Cell. Elsevier BV; 2010;142:967–80.

31. Vosnakis N, Koch M, Scheer E, Kessler P, Mély Y, Didier P, et al. Coactivators and general transcription factors have two distinct dynamic populations dependent on transcription. EMBO J. 2017;36:2710–25.

32. Espinola-Lopez JM, Tan S. The Ada2/Ada3/Gcn5/Sgf29 histone acetyltransferase module. Biochim Biophys Acta Gene Regul Mech. 2021;1864:194629.

33. Kustatscher G, Wills KLH, Furlan C, Rappsilber J. Chromatin enrichment for proteomics. Nat Protoc. 2014;9:2090–9.

34. Goel S, Bergholz JS, Zhao JJ. Targeting CDK4 and CDK6 in cancer. Nat Rev Cancer. Springer Science and Business Media LLC; 2022;22:356–72.

35. Liu W-H, Völse K, Senft D, Jeremias I. A reporter system for enriching CRISPR/Cas9 knockout cells in technically challenging settings like patient models. Sci Rep. 2021;11:12649.

36. Sanders SL, Jennings J, Canutescu A, Link AJ, Weil PA. Proteomics of the eukaryotic transcription machinery: identification of proteins associated with

components of yeast TFIID by multidimensional mass spectrometry. Mol Cell Biol. 2002;22:4723–38.

37. Baker SP, Grant PA. The SAGA continues: expanding the cellular role of a transcriptional co-activator complex. Oncogene. 2007;26:5329–40.

38. Rodríguez-Navarro S. Insights into SAGA function during gene expression [Internet]. EMBO reports. 2009. page 843–50. Available from: http://dx.doi.org/10.1038/embor.2009.168

39. Kurabe, Katagiri, Komiya, Ito, Sugiyama. … expression of a novel component of TFTC/STAGA histone acetyltransferase complexes, rat SGF29, in hepatocellular carcinoma: possible implication for the …. Oncogene [Internet]. Available from: https://idp.nature.com/authorize/casa?redirect_uri=https://www.nature.com/articles/1210349&casa_token=XgPzaJbobnUAAAAA:lA9MpQAJUUvIhfme7uEFqXMcJfAucnj0Ye0OlA-lv7KZTigixkGUarIgvfbDMOXEs0PPPE3wpWz_9ht_

40. Chen B-R, Deshpande A, Barbosa K, Kleppe M, Lei X, Yeddula N, et al. A JAK/STAT-mediated inflammatory signaling cascade drives oncogenesis in AF10-rearranged AML. Blood. American Society of Hematology; 2021;137:3403–15.

41. Li W, Köster J, Xu H, Chen CH, Xiao T, Liu JS, et al. Quality control, modeling, and visualization of CRISPR screens with MAGeCK-VISPR. Genome Biol. 2015;16:281.

42. Wang B, Wang M, Zhang W, Xiao T, Chen CH, Wu A, et al. Integrative analysis of pooled CRISPR genetic screens using MAGeCKFlute. Nat Protoc. 2019;14:756–80.

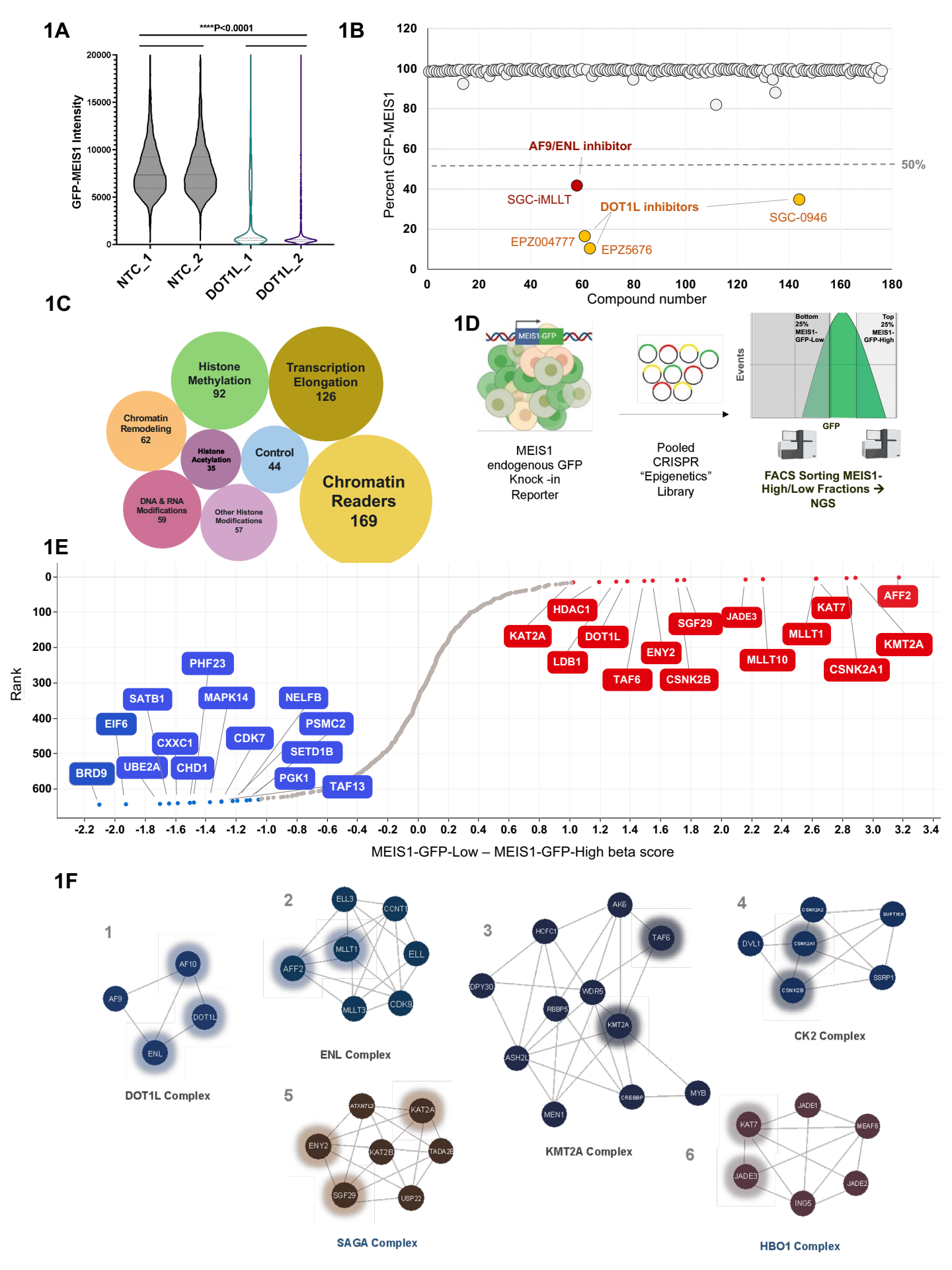
1A
****P<0.0001
GFP-MEIS1 Intensity
20000
15000
10000
5000
0
NTC_1
NTC_2
DOT1L_1
DOT1L_2
1B
Percent GFP-MEIS1
Compound number
AF9/ENL inhibitor
SGC-iMLLT
DOT1L inhibitors
SGC-0946
EPZ004777
EPZ5676
50%
1C
Histone Methylation 92
Transcription Elongation 126
Chromatin Remodeling 62
Histone Acetylation 35
Control 44
DNA & RNA Modifications 59
Other Histone Modifications 57
Chromatin Readers 169
1D
MEIS1-GFP
MEIS1 endogenous GFP Knock -in Reporter
Pooled CRISPR "Epigenetics" Library
Events
Bottom 25% MEIS1-GFP-Low
Top 25% MEIS1-GFP-High
GFP
FACS Sorting MEIS1-High/Low Fractions → NGS
1E
Rank
HDAC1
KAT2A
DOT1L
LDB1
ENY2
TAF6
CSNK2B
SGF29
JADE3
MLLT10
MLLT1
KAT7
CSNK2A1
AFF2
KMT2A
PHF23
SATB1
MAPK14
NELFB
EIF6
PSMC2
CXXC1
CDK7
SETD1B
BRD9
UBE2A
CHD1
PGK1
TAF13
MEIS1-GFP-Low – MEIS1-GFP-High beta score
1F
1
AF10
AF9
DOT1L
ENL
DOT1L Complex
2
ELL3
CCNT1
MLLT1
ELL
AFF2
MLLT3
CDK9
ENL Complex
3
AK6
HCFC1
TAF6
DPY30
WDR5
RBBP5
KMT2A
ASH2L
CREBBP
MYB
MEN1
KMT2A Complex
4
CSNK2A2
SUPT16H
DVL1
CSNK2A1
SSRP1
CSNK2B
CK2 Complex
5
ATXN7L3
KAT2A
ENY2
KAT2B
TADA2B
SGF29
USP22
SAGA Complex
6
JADE1
KAT7
MEAF6
JADE3
JADE2
ING5
HBO1 Complex

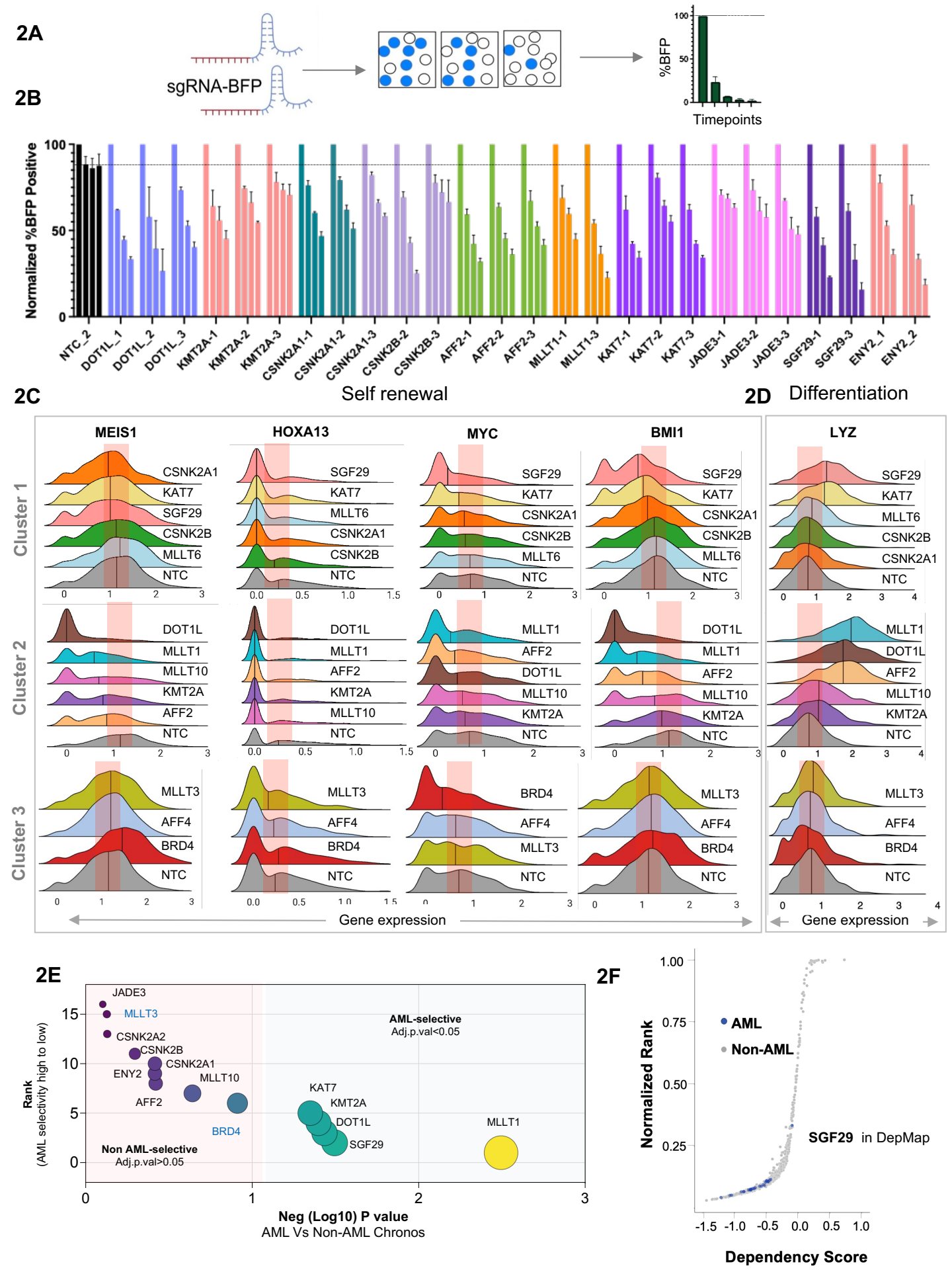
2A
sgRNA-BFP
%BFP
Timepoints
2B
Normalized %BFP Positive
NTC_2
DOT1L_1
DOT1L_2
DOT1L_3
KMT2A-1
KMT2A-2
KMT2A-3
CSNK2A1-1
CSNK2A1-2
CSNK2A1-3
CSNK2B-2
CSNK2B-3
AFF2-1
AFF2-2
AFF2-3
MLLT1-1
MLLT1-3
KAT7-1
KAT7-2
KAT7-3
JADE3-1
JADE3-2
JADE3-3
SGF29-1
SGF29-3
ENY2_1
ENY2_2
Self renewal
2C
2D
Differentiation
MEIS1
HOXA13
MYC
BMI1
LYZ
Cluster 1
Cluster 2
Cluster 3
Gene expression
2E
JADE3
MLLT3
CSNK2A2
CSNK2B
CSNK2A1
ENY2
MLLT10
AFF2
BRD4
KAT7
KMT2A
DOT1L
SGF29
MLLT1
AML-selective
Adj.p.val<0.05
Non AML-selective
Adj.p.val>0.05
Rank
(AML selectivity high to low)
Neg (Log10) P value
AML Vs Non-AML Chronos
2F
AML
Non-AML
SGF29 in DepMap
Normalized Rank
Dependency Score

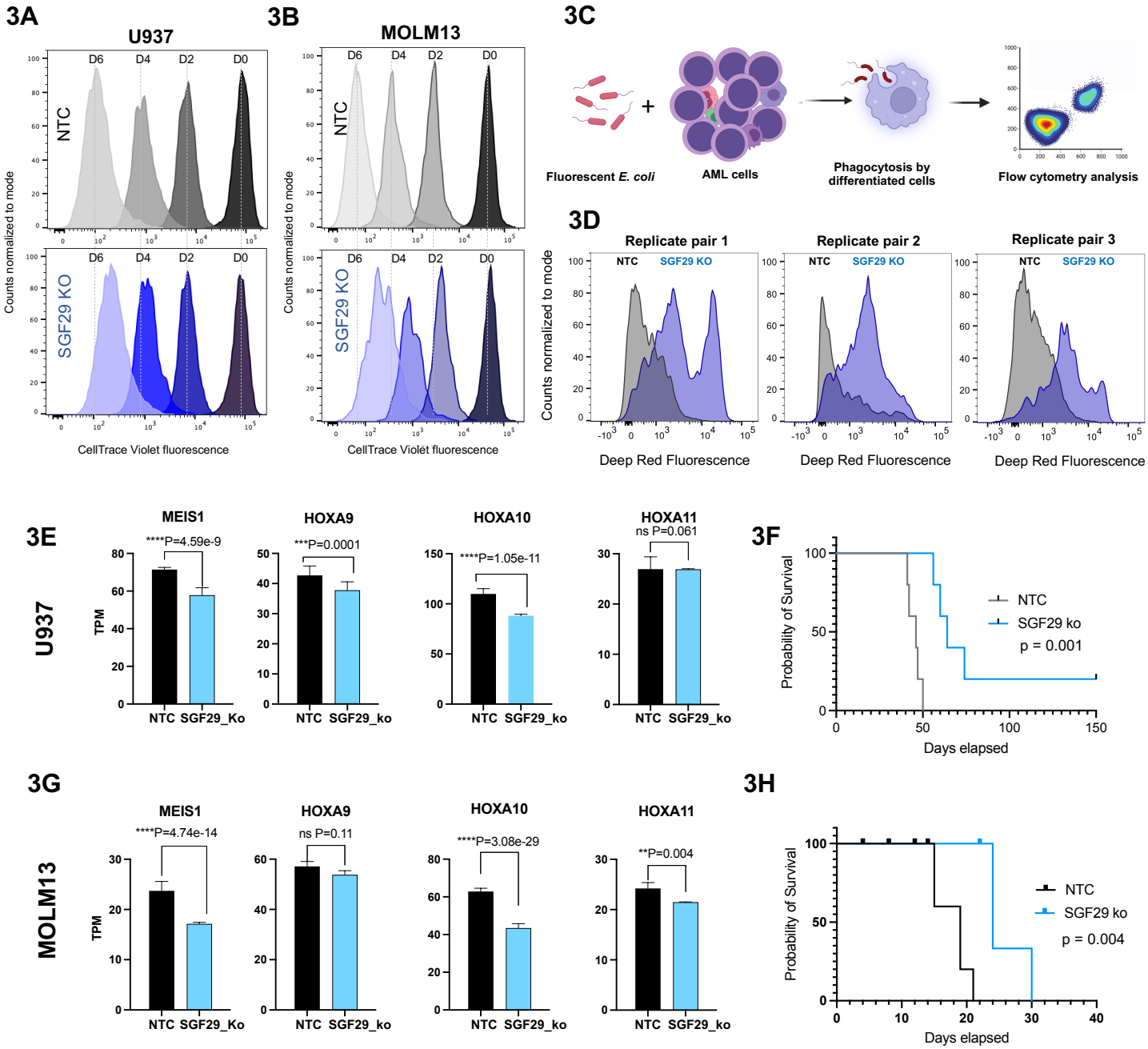
3A
U937
D6
D4
D2
D0
NTC
SGF29 KO
Counts normalized to mode
CellTrace Violet fluorescence
3B
MOLM13
3C
Fluorescent E. coli
AML cells
Phagocytosis by differentiated cells
Flow cytometry analysis
3D
Replicate pair 1
Replicate pair 2
Replicate pair 3
Deep Red Fluorescence
3E
U937
MEIS1
****P=4.59e-9
HOXA9
***P=0.0001
HOXA10
****P=1.05e-11
HOXA11
ns P=0.061
TPM
NTC
SGF29_Ko
SGF29_ko
3F
Probability of Survival
Days elapsed
NTC
SGF29 ko
p = 0.001
3G
MOLM13
MEIS1
****P=4.74e-14
HOXA9
ns P=0.11
HOXA10
****P=3.08e-29
HOXA11
**P=0.004
3H
Probability of Survival
Days elapsed
NTC
SGF29 ko
p = 0.004

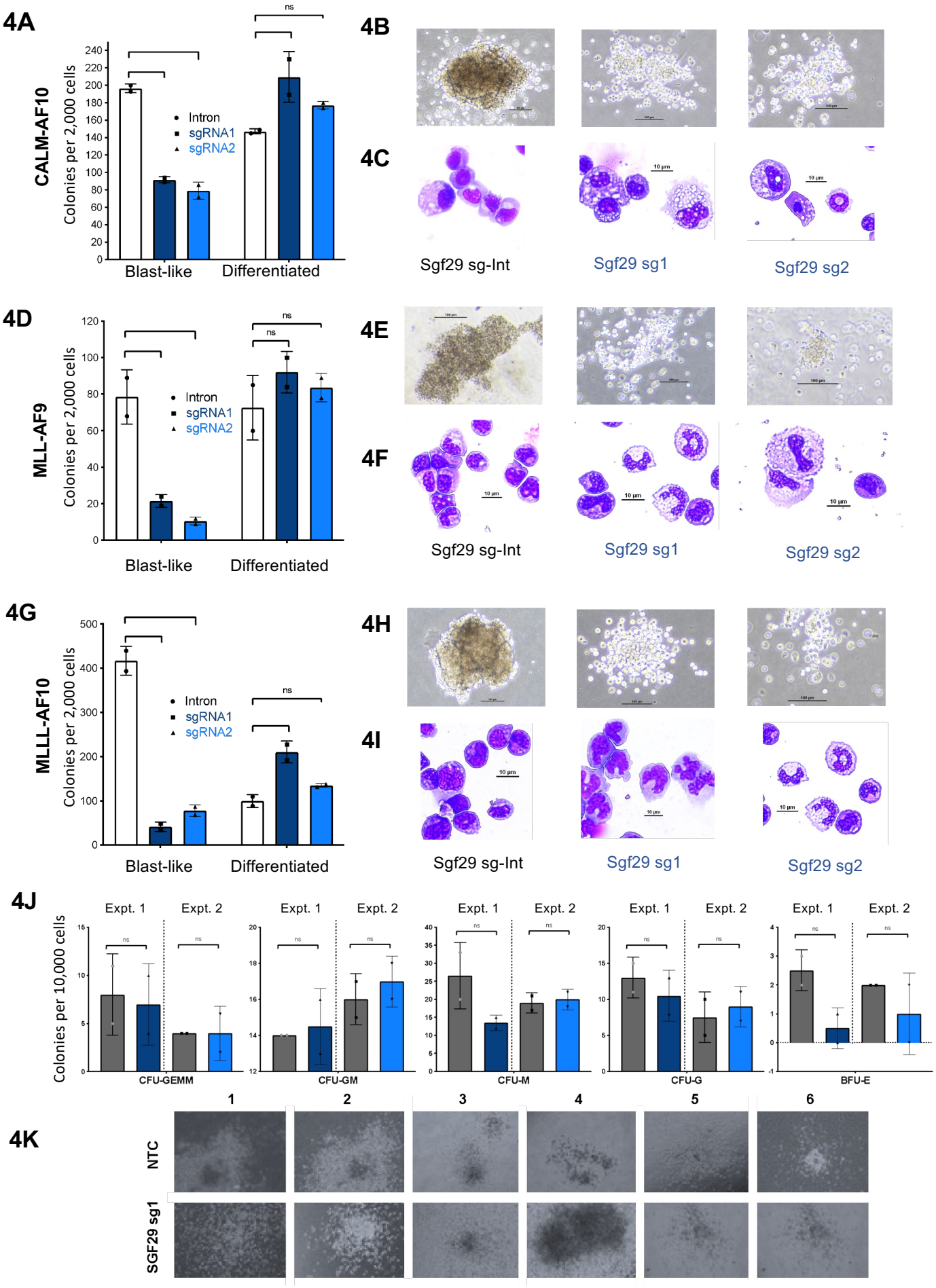
4A
CALM-AF10
Colonies per 2,000 cells
Intron
sgRNA1
sgRNA2
ns
Blast-like
Differentiated
4B
4C
Sgf29 sg-Int
Sgf29 sg1
Sgf29 sg2
4D
MLL-AF9
Colonies per 2,000 cells
Intron
sgRNA1
sgRNA2
ns
Blast-like
Differentiated
4E
4F
Sgf29 sg-Int
Sgf29 sg1
Sgf29 sg2
4G
MLLL-AF10
Colonies per 2,000 cells
Intron
sgRNA1
sgRNA2
ns
Blast-like
Differentiated
4H
4I
Sgf29 sg-Int
Sgf29 sg1
Sgf29 sg2
4J
Colonies per 10,000 cells
Expt. 1
Expt. 2
ns
CFU-GEMM
CFU-GM
CFU-M
CFU-G
BFU-E
4K
1
2
3
4
5
6
NTC
SGF29 sg1

5A

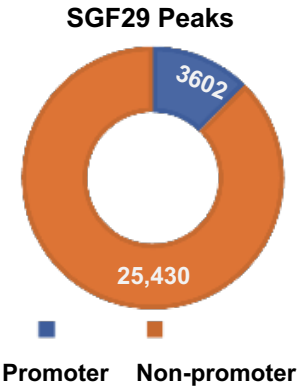
SGF29 Peaks
3602
25,430
Promoter
Non-promoter

5B

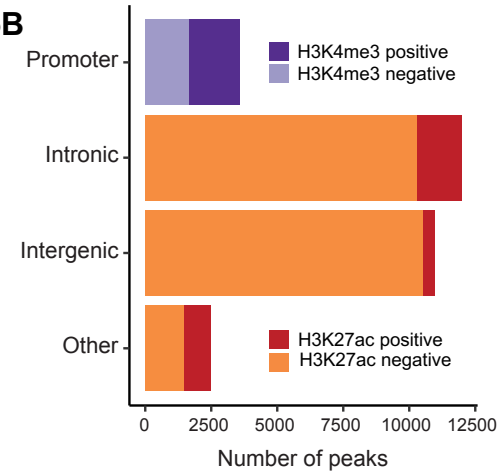
Promoter
Intronic
Intergenic
Other
H3K4me3 positive
H3K4me3 negative
H3K27ac positive
H3K27ac negative
0
2500
5000
7500
10000
12500
Number of peaks

5C

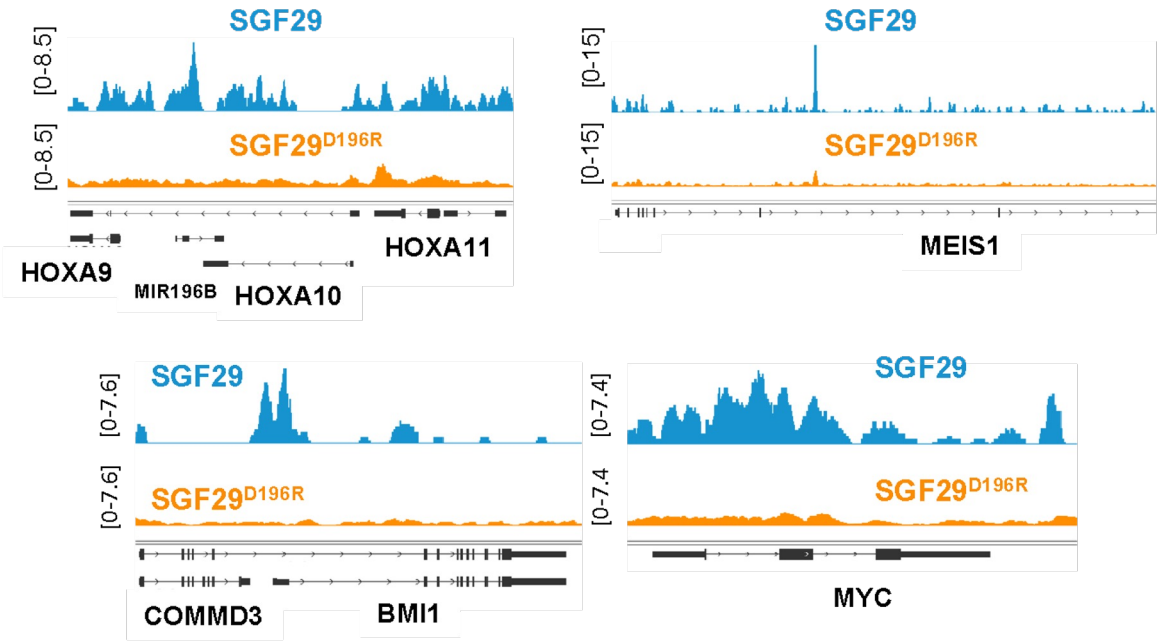
SGF29
[0-8.5]
SGF29D196R
[0-8.5]
HOXA9
MIR196B
HOXA10
HOXA11
SGF29
[0-15]
SGF29D196R
[0-15]
MEIS1
SGF29
[0-7.6]
SGF29D196R
[0-7.6]
COMMD3
BMI1
SGF29
[0-7.4]
SGF29D196R
[0-7.4
MYC

5D

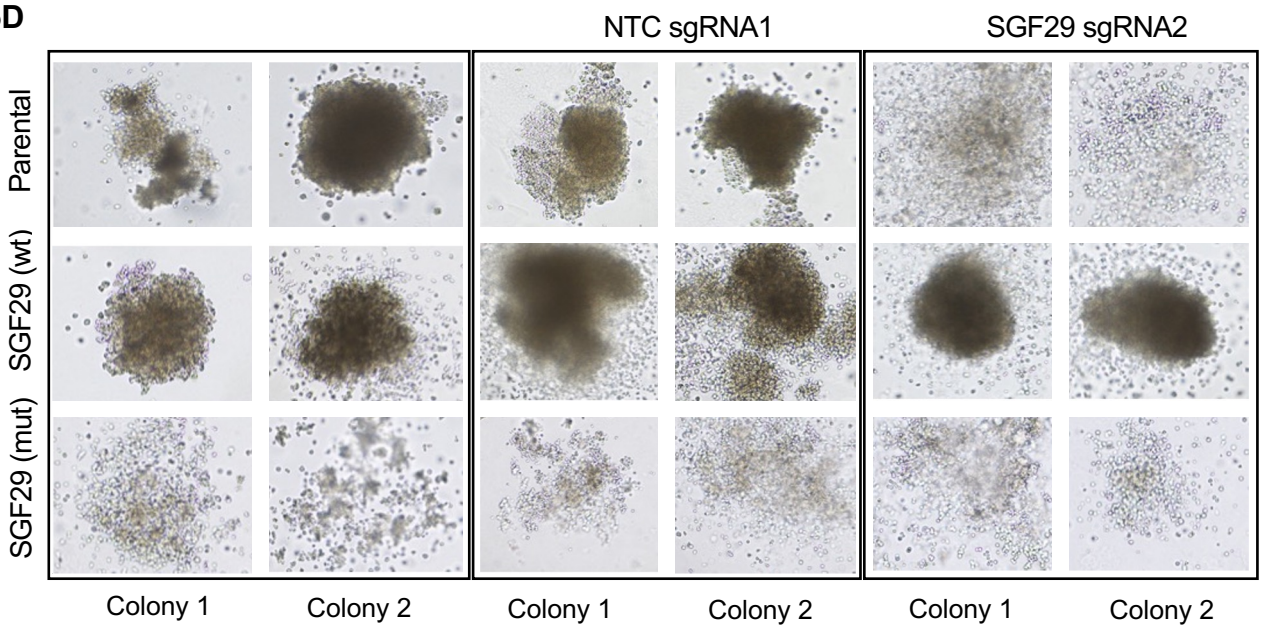
NTC sgRNA1
SGF29 sgRNA2
Parental
SGF29 (wt)
SGF29 (mut)
Colony 1
Colony 2
Colony 1
Colony 2
Colony 1
Colony 2

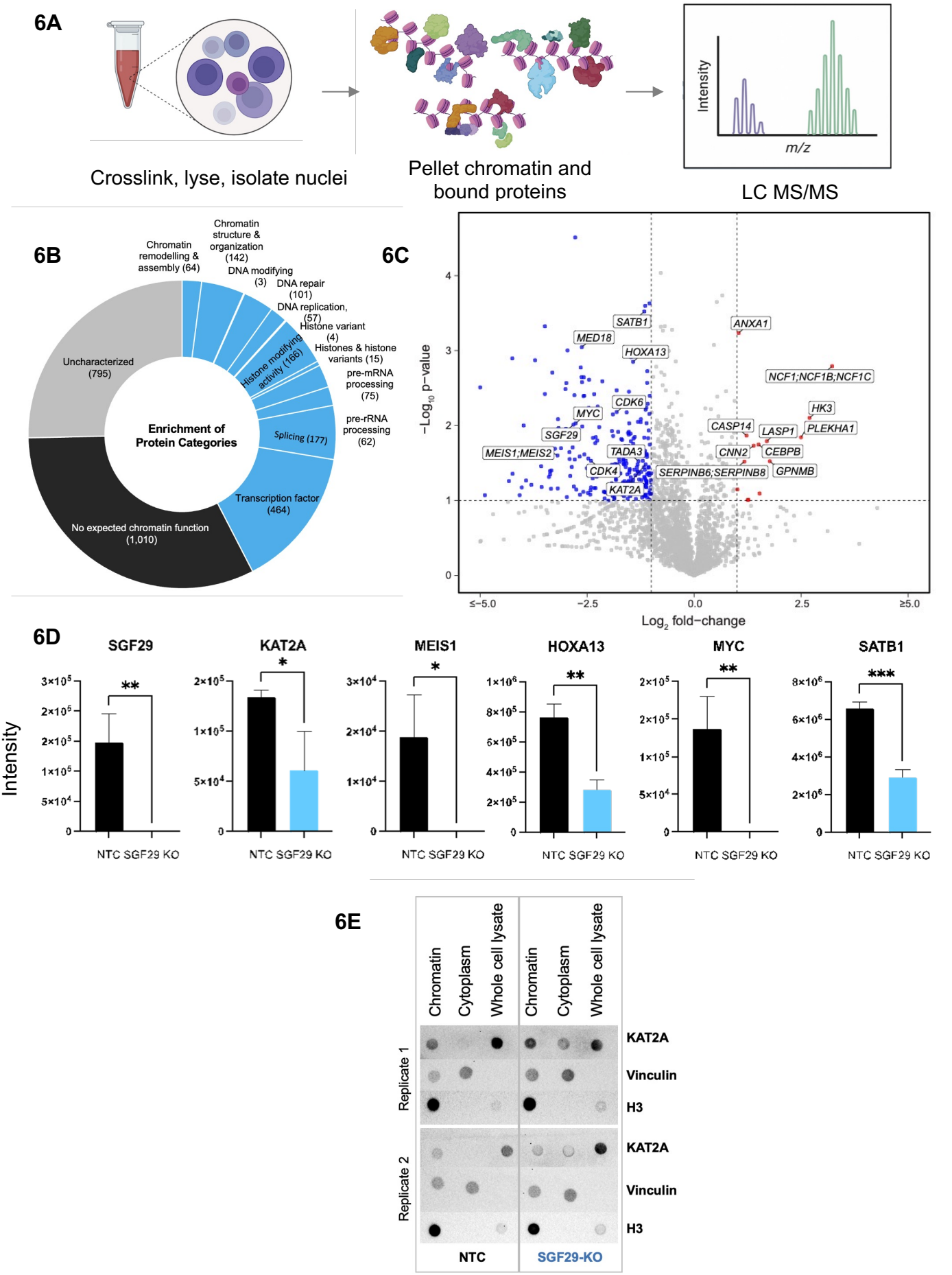
6A
Crosslink, lyse, isolate nuclei
Pellet chromatin and bound proteins
Intensity
m/z
LC MS/MS
6B
Enrichment of Protein Categories
Chromatin remodelling & assembly (64)
Chromatin structure & organization (142)
DNA modifying (3)
DNA repair (101)
DNA replication, (57)
Histone variant (4)
Histones & histone variants (15)
pre-mRNA processing (75)
pre-rRNA processing (62)
Splicing (177)
Transcription factor (464)
No expected chromatin function (1,010)
Uncharacterized (795)
Histone modifying activity (166)
6C
−Log10 p−value
Log2 fold−change
SATB1
MED18
HOXA13
ANXA1
NCF1;NCF1B;NCF1C
CDK6
MYC
HK3
CASP14
LASP1
PLEKHA1
SGF29
MEIS1;MEIS2
TADA3
CNN2
CEBPB
CDK4
SERPINB6;SERPINB8
GPNMB
KAT2A
6D
SGF29
KAT2A
MEIS1
HOXA13
MYC
SATB1
Intensity
NTC SGF29 KO
6E
Chromatin
Cytoplasm
Whole cell lysate
Replicate 1
Replicate 2
KAT2A
Vinculin
H3
NTC
SGF29-KO

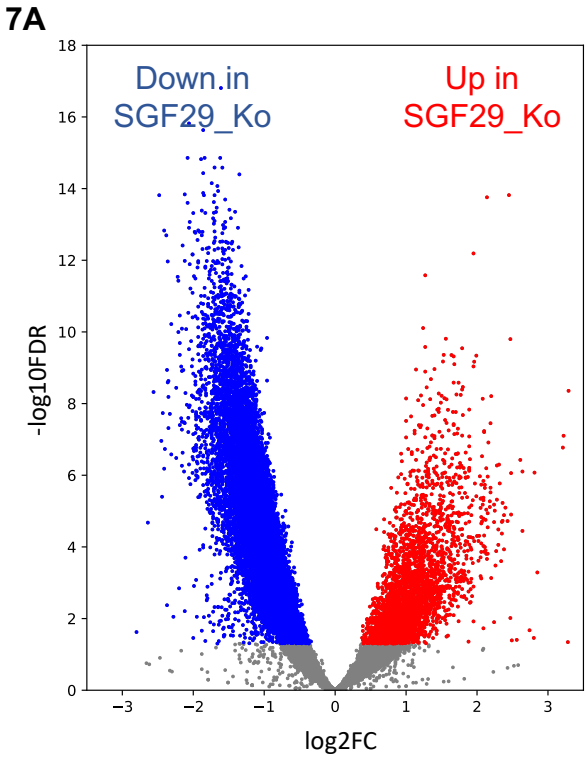
7A
Down in SGF29_Ko
Up in SGF29_Ko
-log10FDR
log2FC

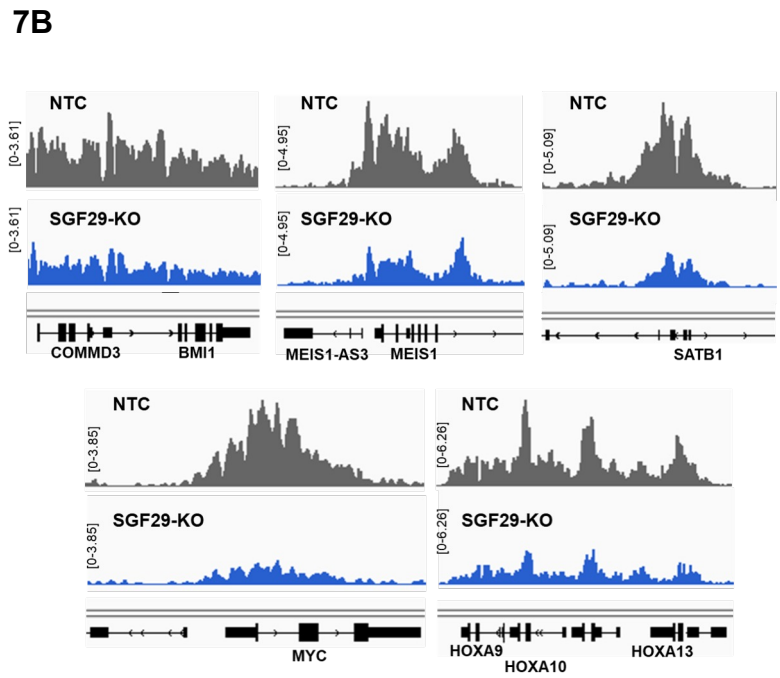
7B
NTC
SGF29-KO
COMMD3
BMI1
MEIS1-AS3
MEIS1
SATB1
MYC
HOXA9
HOXA10
HOXA13

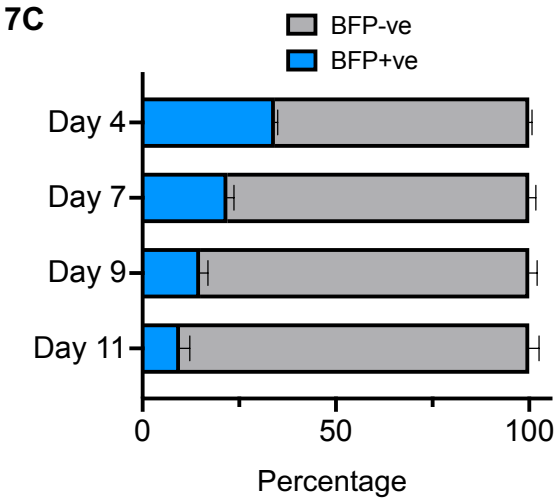
7C
BFP-ve
BFP+ve
Day 4
Day 7
Day 9
Day 11
Percentage

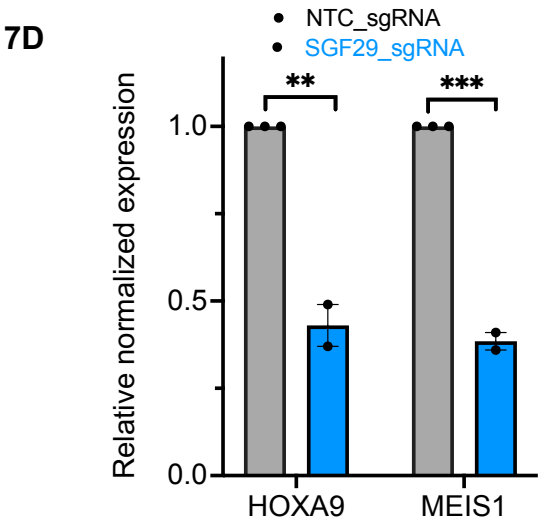
7D
NTC_sgRNA
SGF29_sgRNA
Relative normalized expression
HOXA9
MEIS1

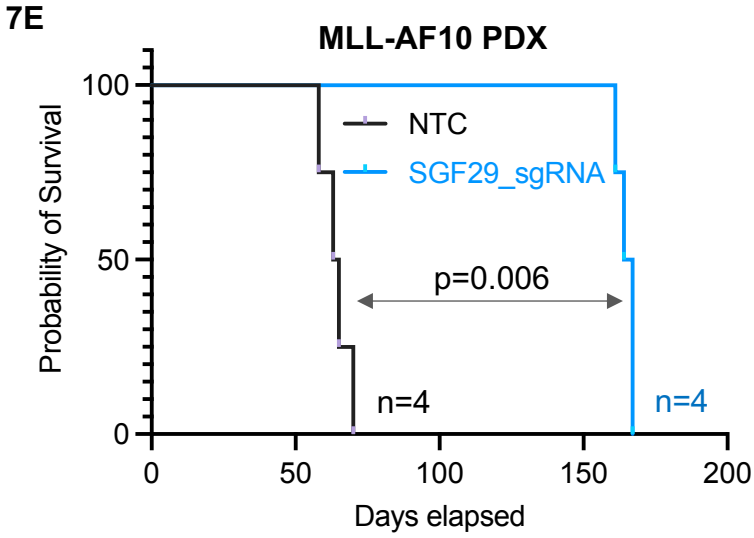
7E
MLL-AF10 PDX
NTC
SGF29_sgRNA
p=0.006
n=4
n=4
Probability of Survival
Days elapsed

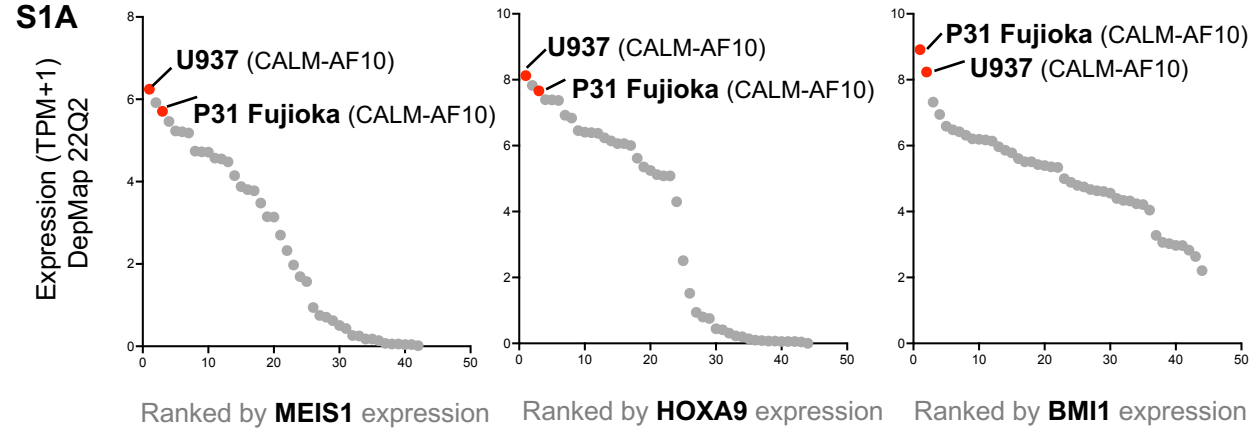
S1A
Expression (TPM+1) DepMap 22Q2
U937 (CALM-AF10)
P31 Fujioka (CALM-AF10)
Ranked by MEIS1 expression
Ranked by HOXA9 expression
Ranked by BMI1 expression

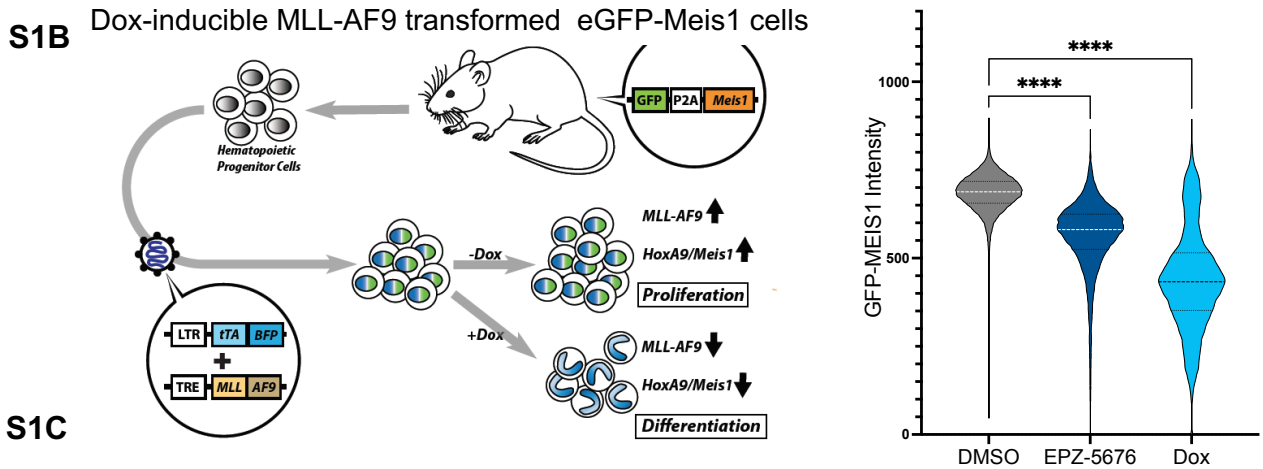
S1B
Dox-inducible MLL-AF9 transformed eGFP-Meis1 cells
Hematopoietic Progenitor Cells
GFP
P2A
Meis1
LTR
tTA
BFP
TRE
MLL
AF9
-Dox
+Dox
MLL-AF9
HoxA9/Meis1
Proliferation
Differentiation
GFP-MEIS1 Intensity
****
****
DMSO
EPZ-5676
Dox

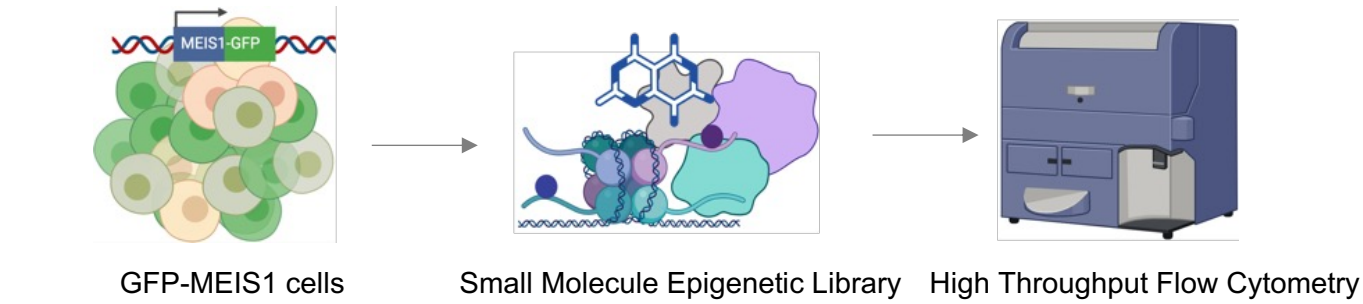
S1C
MEIS1-GFP
GFP-MEIS1 cells
Small Molecule Epigenetic Library
High Throughput Flow Cytometry

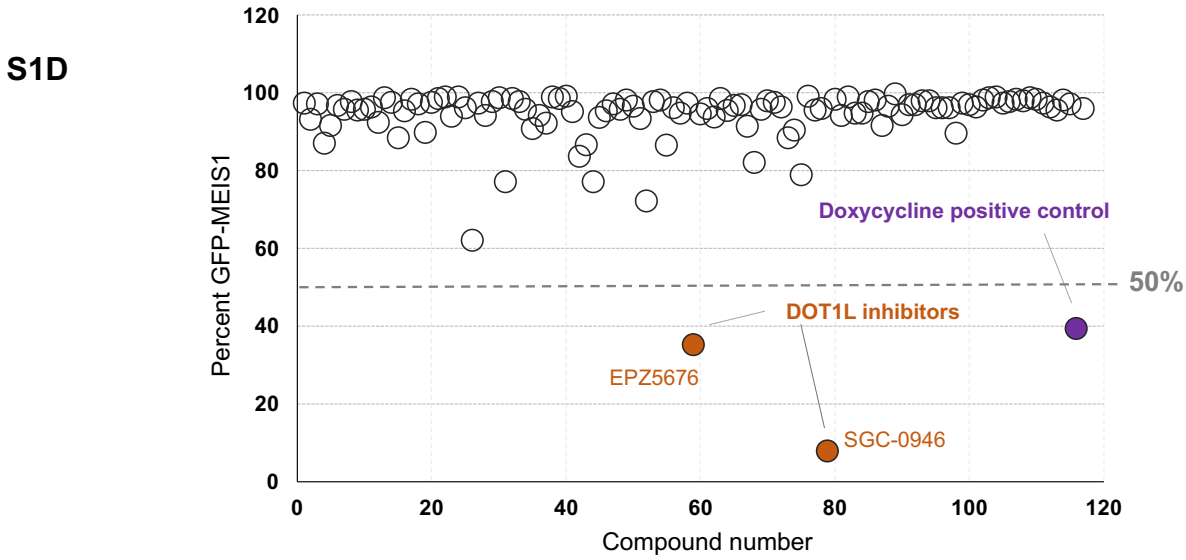
S1D
Percent GFP-MEIS1
Compound number
Doxycycline positive control
50%
DOT1L inhibitors
EPZ5676
SGC-0946

S2A

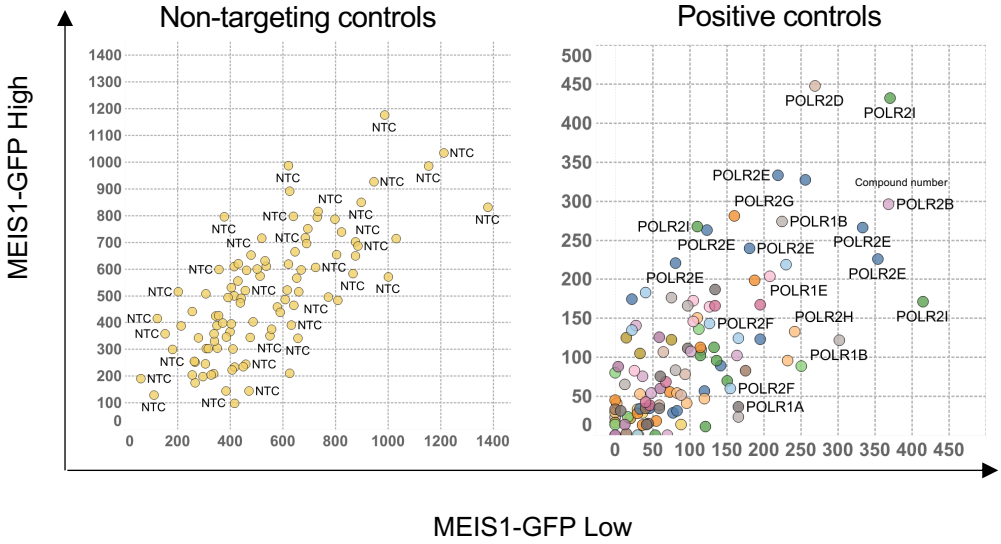
Non-targeting controls
Positive controls
MEIS1-GFP High
MEIS1-GFP Low
NTC
POLR2D
POLR2I
POLR2E
POLR2G
POLR2B
POLR1B
POLR1E
POLR2F
POLR2H
POLR1A
Compound number

S2B

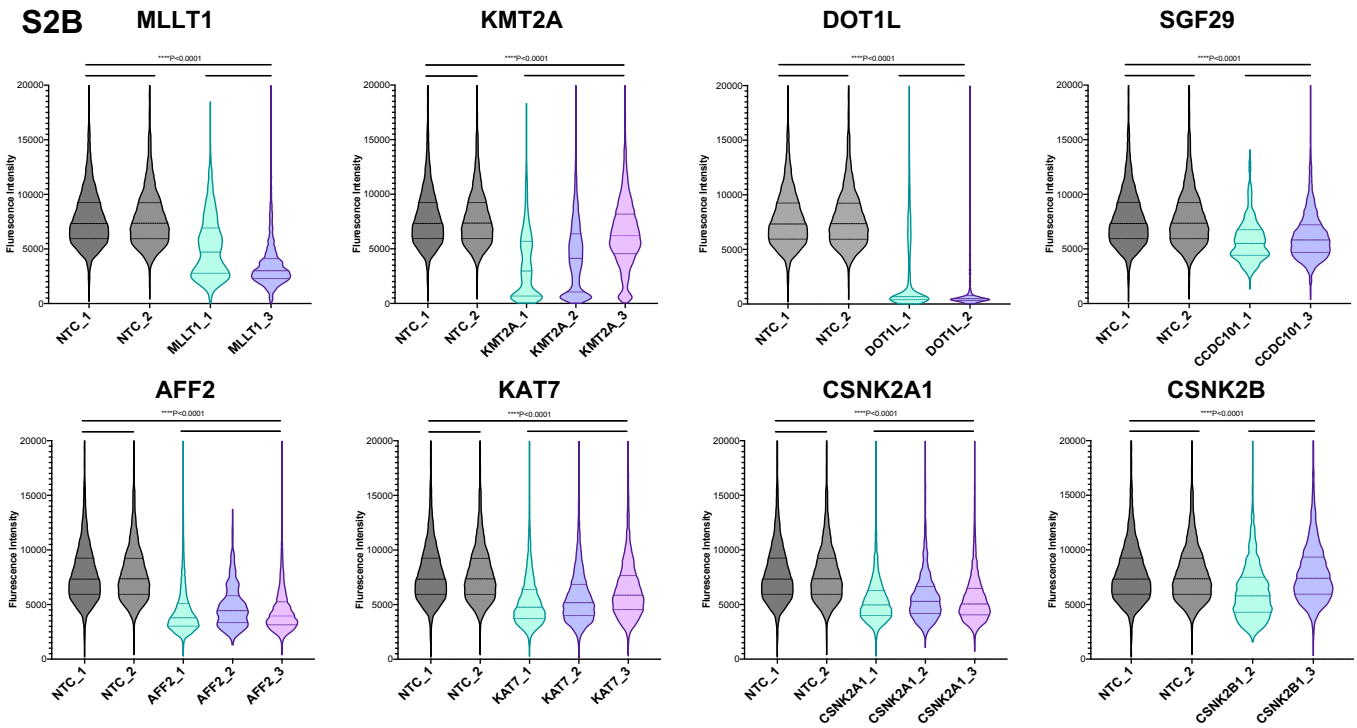
MLLT1
KMT2A
DOT1L
SGF29
AFF2
KAT7
CSNK2A1
CSNK2B
****P<0.0001
Fluorescence Intensity
NTC_1
NTC_2
MLLT1_1
MLLT1_3
KMT2A_1
KMT2A_2
KMT2A_3
DOT1L_1
DOT1L_2
CCDC101_1
CCDC101_3
AFF2_1
AFF2_2
AFF2_3
KAT7_1
KAT7_2
KAT7_3
CSNK2A1_1
CSNK2A1_2
CSNK2A1_3
CSNK2B1_2
CSNK2B1_3

S2C

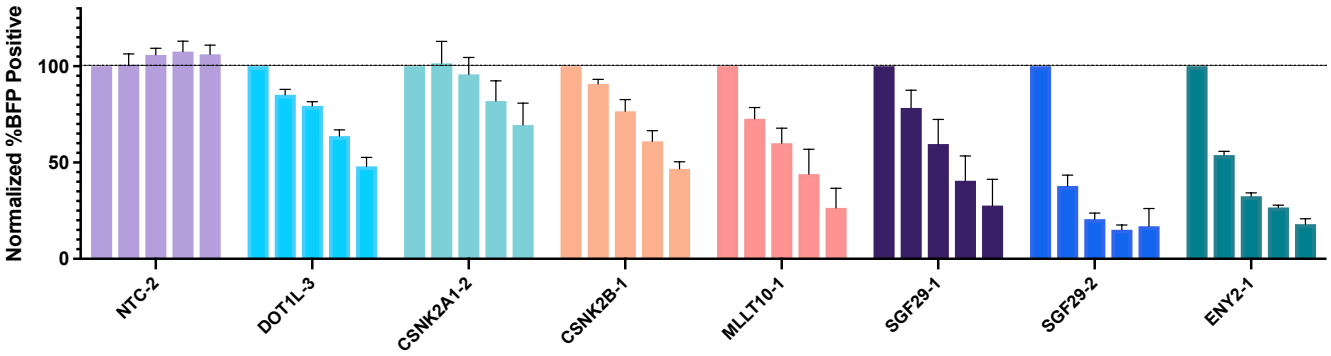
Normalized %BFP Positive
NTC-2
DOT1L-3
CSNK2A1-2
CSNK2B-1
MLLT10-1
SGF29-1
SGF29-2
ENY2-1

S2D

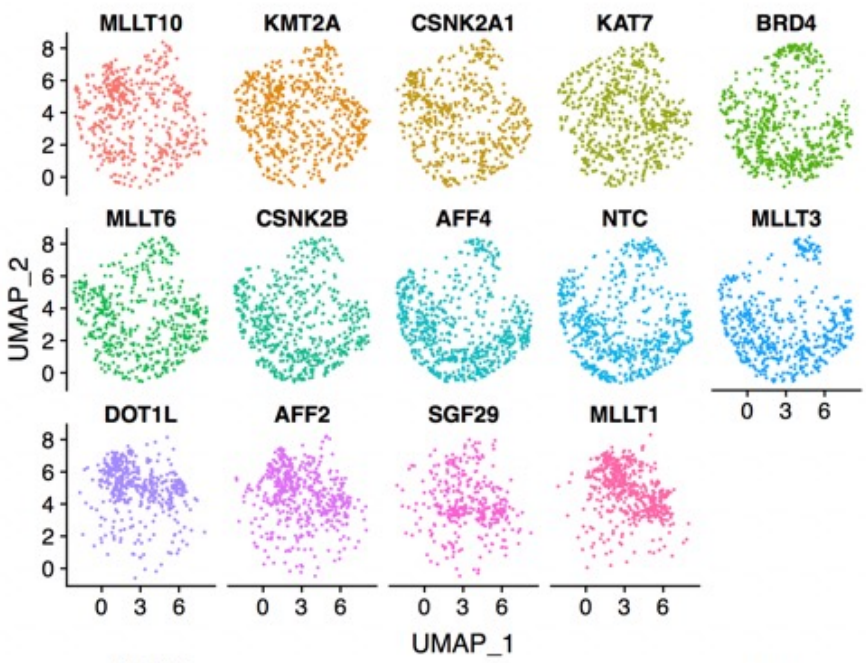

S2E

All genes

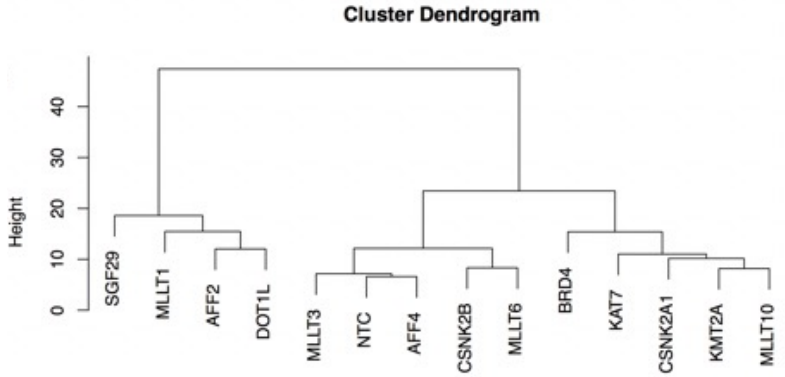

S2F

HOX/MEIS genes

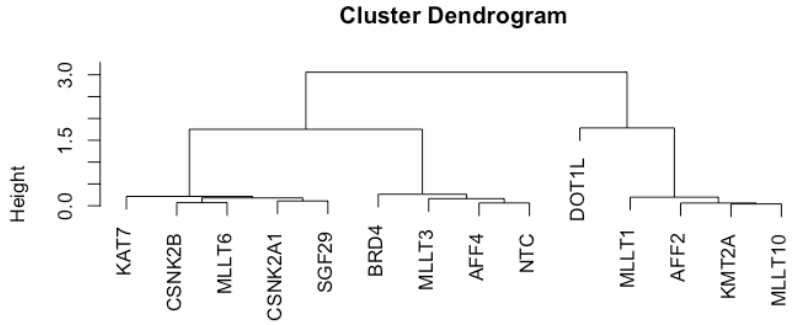

S2G

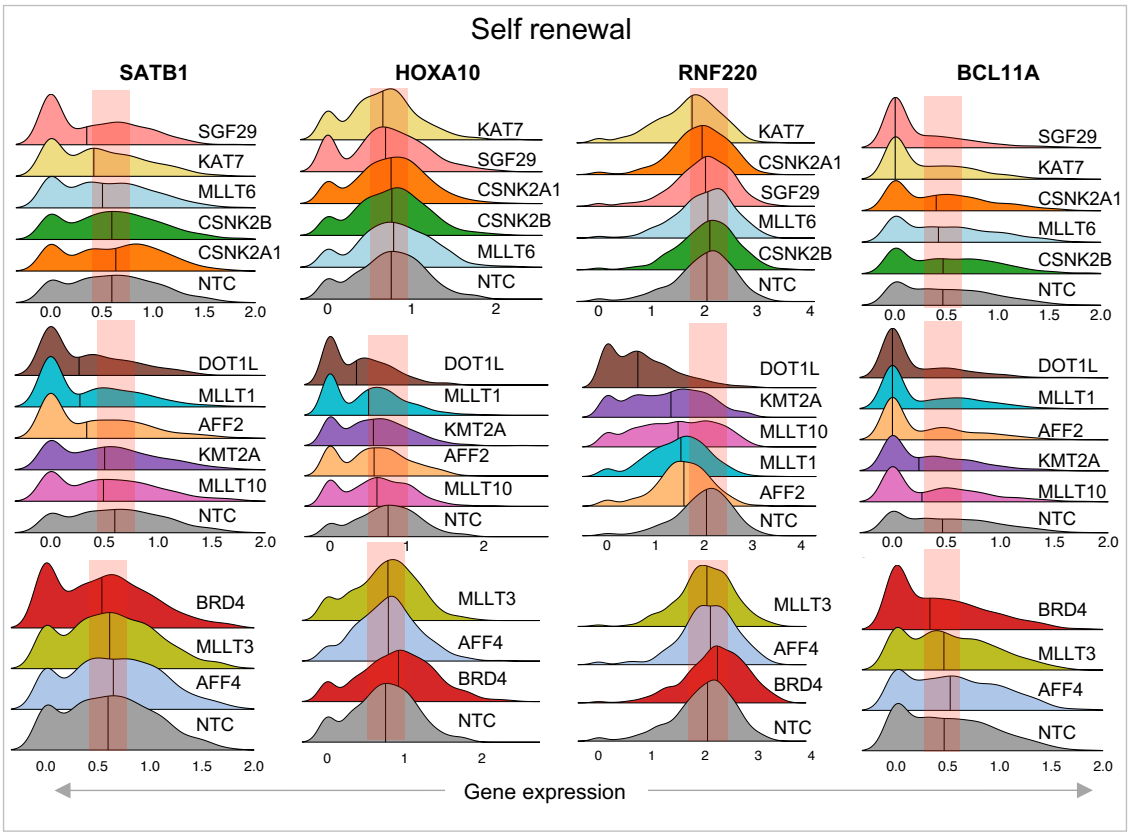
Self renewal
SATB1
HOXA10
RNF220
BCL11A
Cluster 1
Cluster 2
Cluster 3
SGF29
KAT7
MLLT6
CSNK2B
CSNK2A1
NTC
DOT1L
MLLT1
AFF2
KMT2A
MLLT10
BRD4
MLLT3
AFF4
Gene expression

S2H

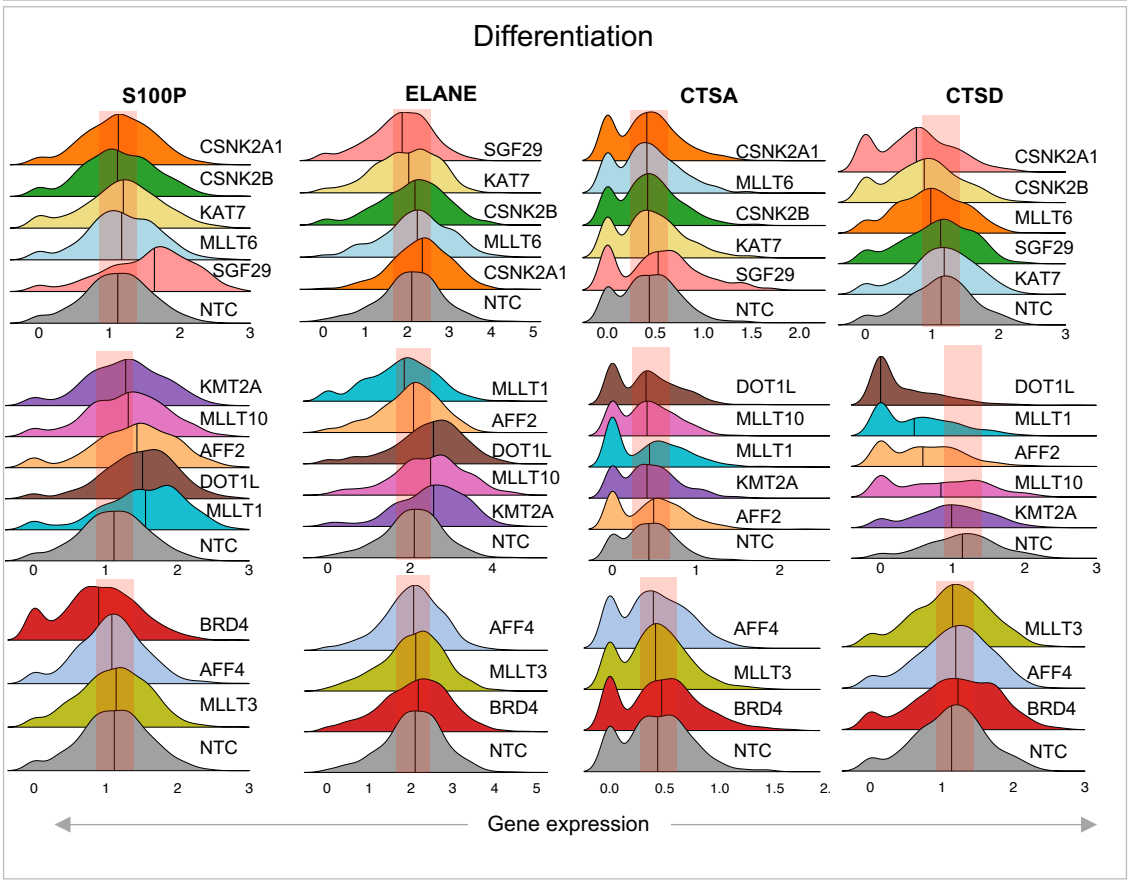
Differentiation
S100P
ELANE
CTSA
CTSD
Cluster 1
Cluster 2
Cluster 3
CSNK2A1
CSNK2B
KAT7
MLLT6
SGF29
NTC
KMT2A
MLLT10
AFF2
DOT1L
MLLT1
BRD4
AFF4
MLLT3
Gene expression

S2I

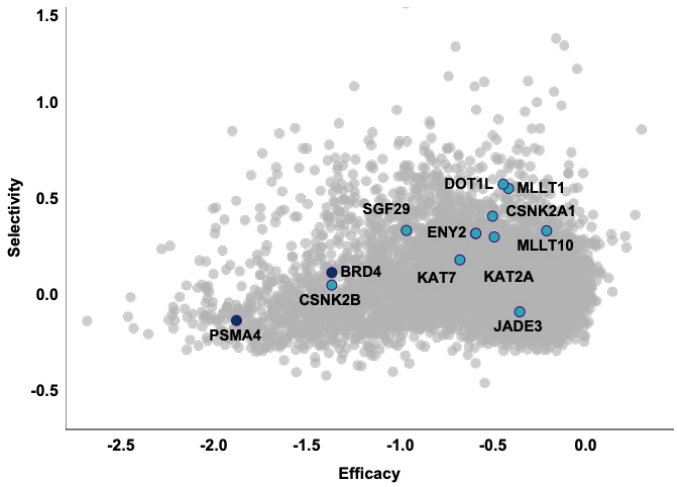

S3A

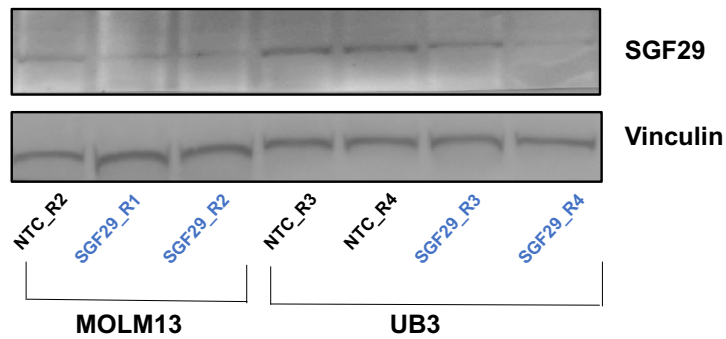

S3B

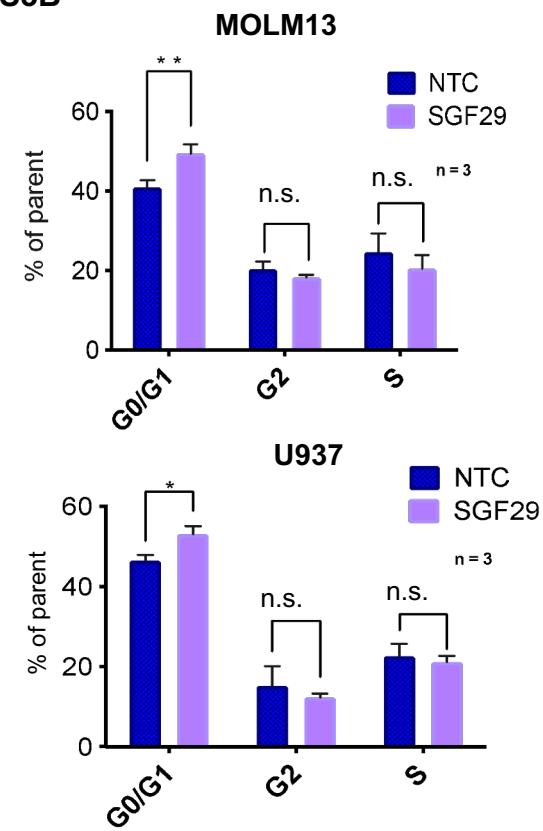

S3C

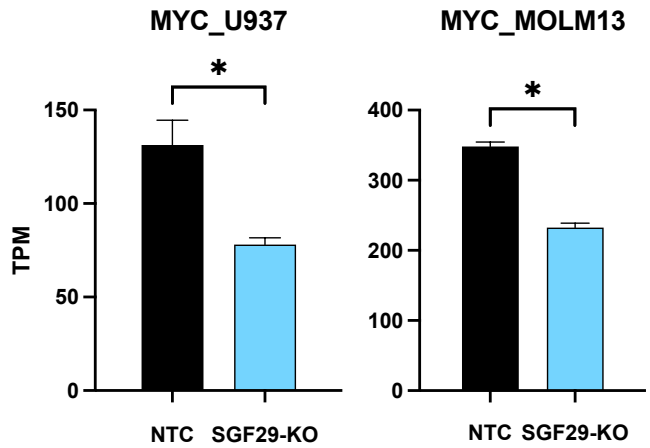

S3D

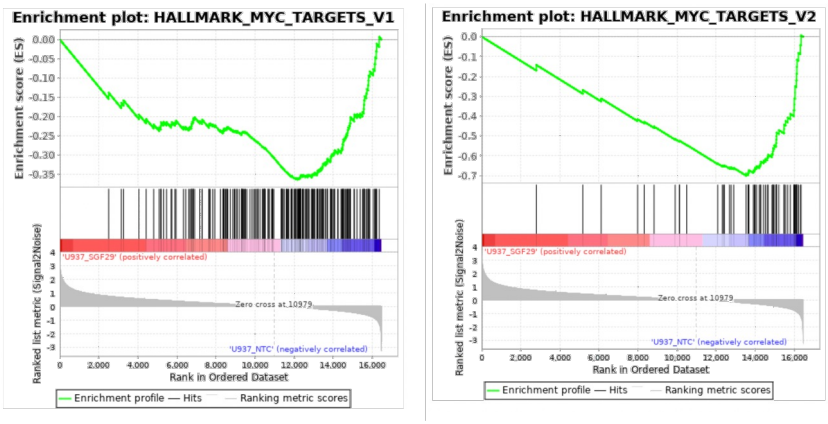

S4A

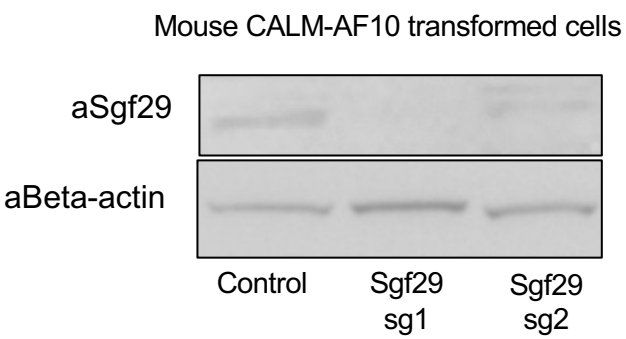

S4B

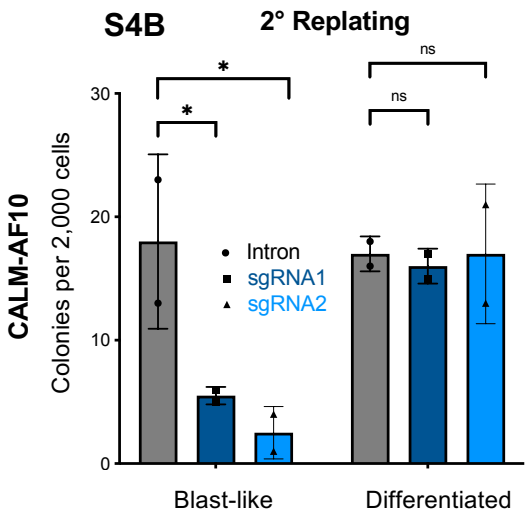

S4C

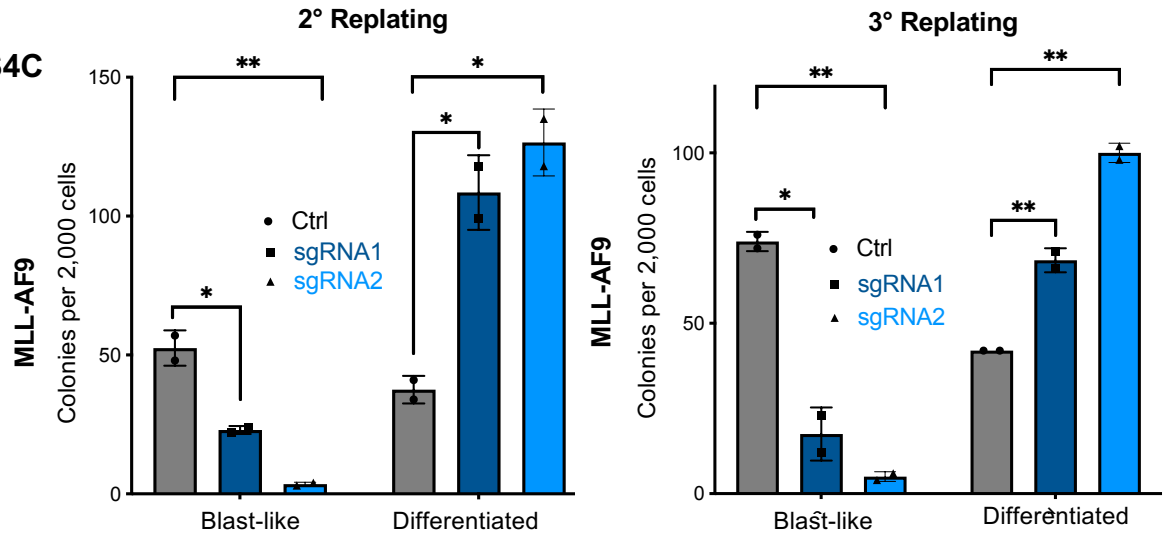

S4D

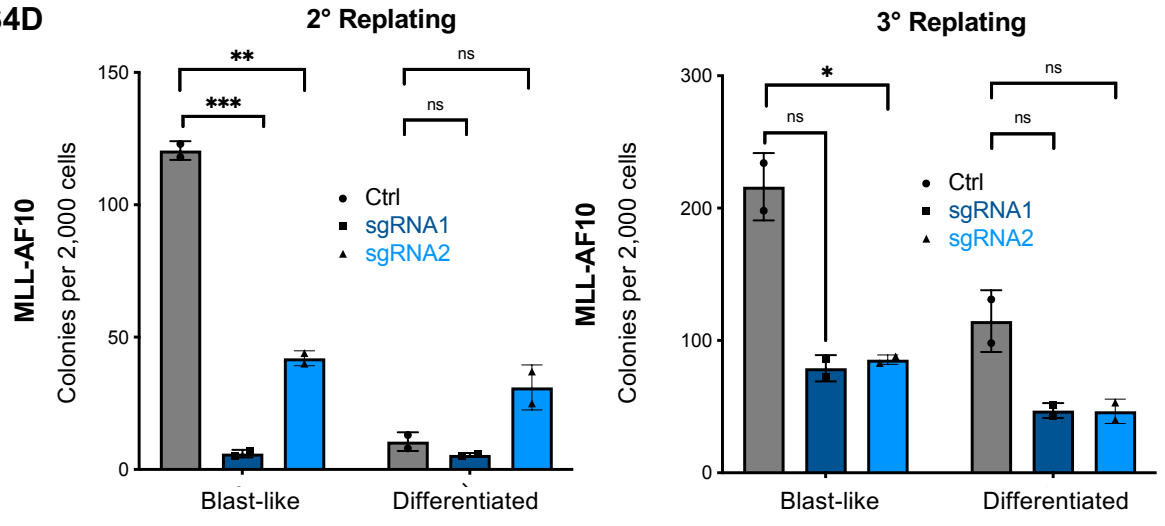

S4E

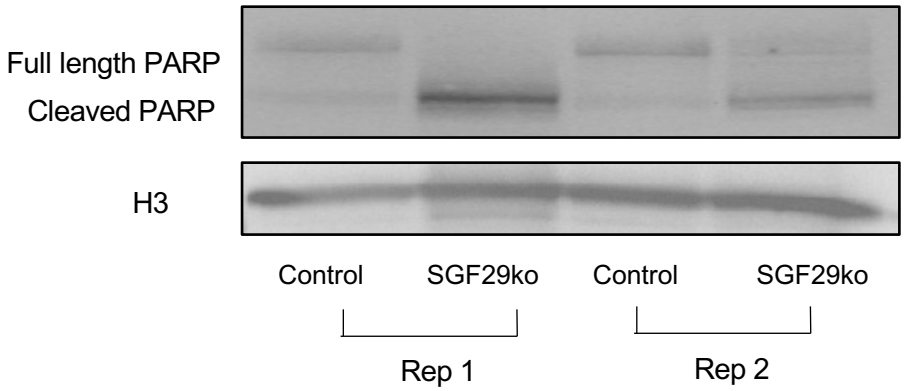
Full length PARP
Cleaved PARP
H3
Control
SGF29ko
Control
SGF29ko
Rep 1
Rep 2

S5A

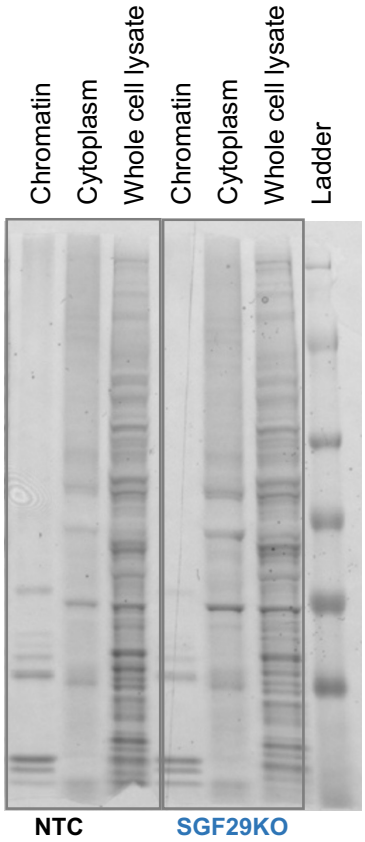
Chromatin
Cytoplasm
Whole cell lysate
Chromatin
Cytoplasm
Whole cell lysate
Ladder
NTC
SGF29KO

S5B

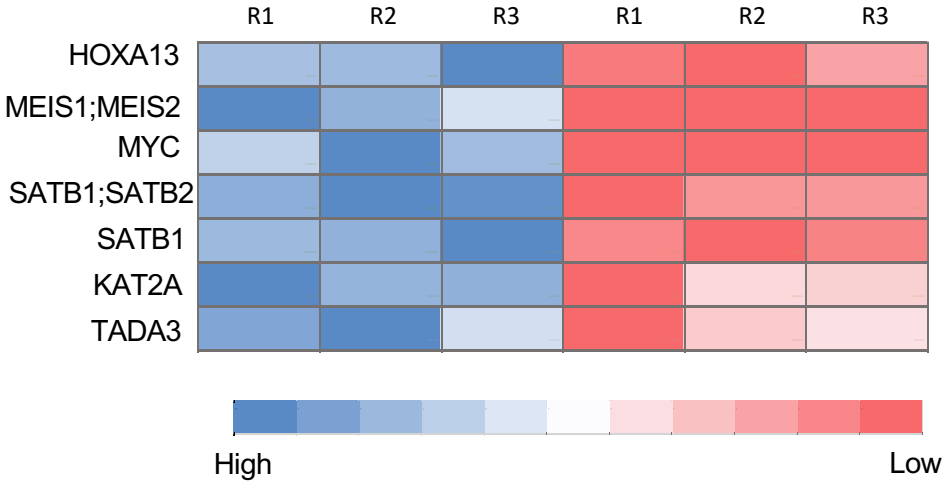
R1
R2
R3
R1
R2
R3
HOXA13
MEIS1;MEIS2
MYC
SATB1;SATB2
SATB1
KAT2A
TADA3
High
Low

S6A

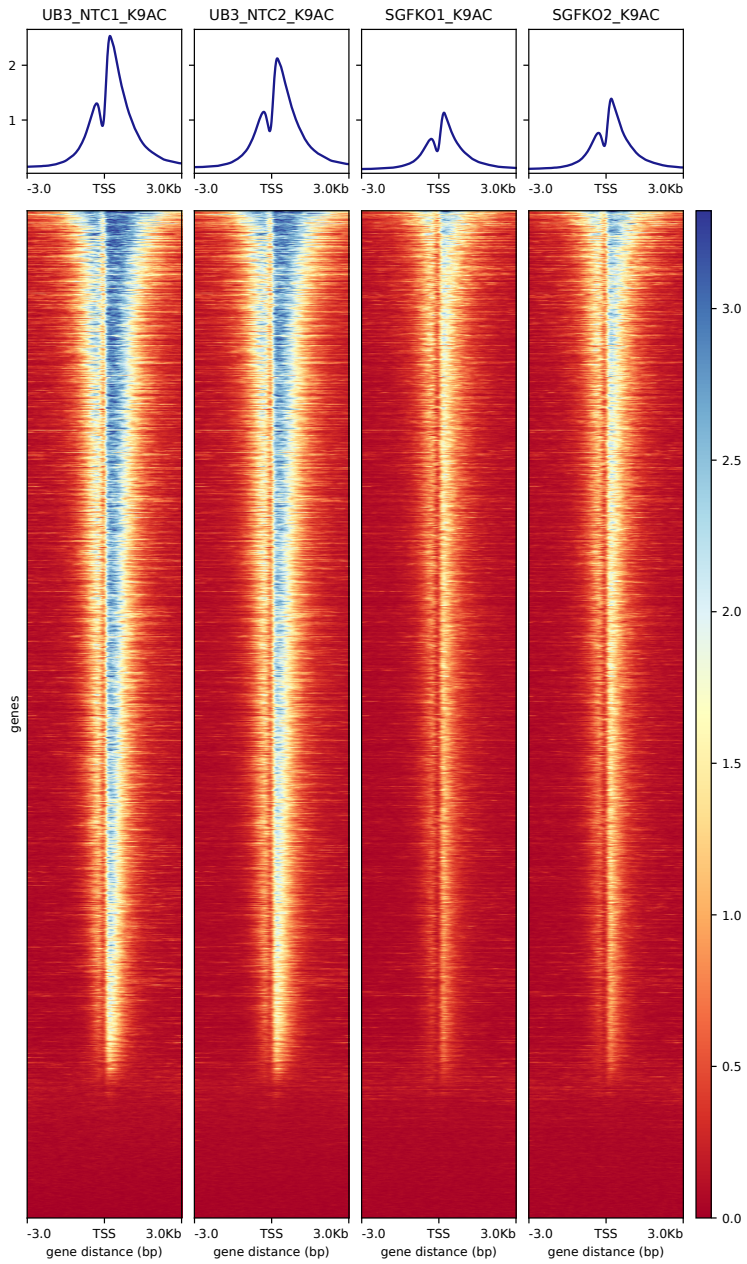
UB3_NTC1_K9AC
UB3_NTC2_K9AC
SGFKO1_K9AC
SGFKO2_K9AC
-3.0
TSS
3.0Kb
gene distance (bp)
genes
3.0
2.5
2.0
1.5
1.0
0.5
0.0

S7A

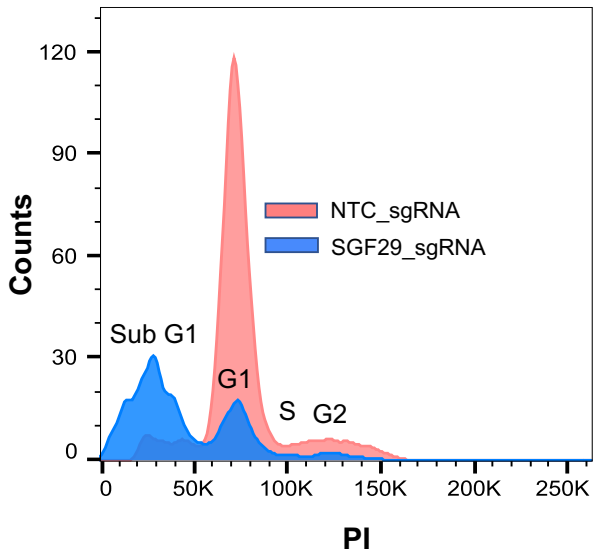
Counts
PI
NTC_sgRNA
SGF29_sgRNA
Sub G1
G1
S
G2
0
30
60
90
120
0
50K
100K
150K
200K
250K

SUPPLEMENTARY FIGURE LEGENDS

Figure S1

Fig. S1A: Expression of indicated genes (MEIS1, HOXA9 and BMI1) in 42 AML cell lines from the DepMap data ranked by expression (x-axis is rank, high to low expression), (y-axis is log transformed transcripts per million (TPM)+1) values.

Fig. S1B: Schematic for generation of inducible Tet-Off MLL-AF9 mouse AML in the GFP-Meis1 background. GFP fluorescence intensity measured upon treatment with DMSO, DOT1L inhibitor, or doxycycline in mouse Tet-Off MLL-AF9 AML (n=3)

Fig S1C: Schematic for phenotypic epigenetics compound screen.

Fig. S2D: Screen results for Tet-Off mouse MLL-AF9 AML; the x-axis indicates % viability on day 5 after treatment with small molecules; the y-axis indicates the percentage of decrease in GFP-Meis1 signal compared to controls. Doxycyline was a positive control that shut off MLL-AF9 expression.

Figure S2

Fig. S2A: sgRNA normalized counts in each sorted fraction (low vs high). Panels depict counts for non-targeting controls and polymerase essential genes, as well as the known HOX/MEIS regulators DOT1L and ENL/MLLT1.

Fig. S2B: Violin plots show the GFP-MEIS fluorescence intensity values plotted on the y-axis from 2-3 unique sgRNAs targeting the indicated genes, compared to 2 non-targeting controls (NTC), measured 7 days after puromycin selection.

Fig. S2C: MOLM13 BFP+ cells over time, normalized to the baseline measurement; the x-axis indicates the sgRNA number for non-targeting controls (NTC) or each gene (n=3). Each bar represents a timepoint measurement: baseline, day 8, day 11, and day 14 for U937; baseline, day 6, day 12, day 18, and day 24 for MOLM13.

Fig.S2D: Uniform Manifold Approximation (UMAP) plots of synthetic gene expression profiles from CROP-Seq perturbations in U937 GFP-MEIS1 cells.

Fig. S2E-F: Hierarchical clustering dendrogram for gene expression of variable features: all genes (**Fig. S2E**) or HOXA-cluster genes and MEIS1 (**Fig. S2F**, see Methods). Branches corresponding to perturbed genes by CRISPR.

Fig. S2G: Ridge plots for CROP-Seq perturbations. Knockout genes are indicated on the y-axis and RNA expression levels for the (**Fig. S2G**) self-renewal-associated genes or (**Fig. S2H**) differentiation-associated genes are on the x-axis. The median expression value is indicated.

Fig. S2I: Selectivity (y-axis) and efficacy (x-axis) analysis for candidate hits in the DepMap data is shown in the scatter plot. PSME4 and BRD4 are included as examples of genes with high efficacy and low selectivity. Each dot in the plot is a gene from the DepMap data. More negative efficacy values indicate higher dependence or fitness score and higher values on the selectivity plot indicates higher differences between fitness scores of sensitive and insensitive cell lines.

Figure S3

Fig. S3A: Western blotting for SGF29 in non-targeting control treated MOLM13 and U937 lysates compared to vinculin is shown as a loading control.

Fig. S3B: Cell cycle progression analysis by propidium iodide staining in human AML cells expressing NTC (blue) or SGF29 (light violset) sgRNAs (n=3).

Fig. S3C: Differences in MYC transcript levels are shown as TPMs on the y-axis in U937 and MOLM13 cells with SGF29 deletion.

Fig. S3D: Hallmarks gene set enrichment analysis (GSEA) for the U937 cell line with SGF29 deletion compared to non-targeting control is shown.

Figure S4

Fig. S4A: Western blot demonstrating loss of SGF29 protein in murine CALM-AF10 leukemia cells transduced with SGF29 sgRNA1 or sgRNA2. Beta Actin as a loading control.

Fig. S4B: Colony forming unit (CFU) assay in murine CALM-AF10 leukemia. 2 nd week of CFU assay showing number of Blast-like as well as differentiated type colonies in cells transduced with intron targeting control or SGF29 targeting sgRNAs. Gray bar indicates cells with Intron whereas Blue bars indicate Sgf29 sgRNA expressing cells. (n=3); ns=non-significant; *=P<0.05.

Fig. S4C: Colony forming unit (CFU) assay in murine MLL-AF9 leukemia cells showing second (left panel) and third (right panel) replating. Gray bars indicate the colonies from cells expressing Intron sgRNA. Blue bars indicate colonies from cells expressing sgRNAs targeting Sgf29. n=3); *=P<0.05; **=P<0.005.

Fig. S4D: Colony forming unit (CFU) assay in murine MLL-AF10 transformed leukemia. The left panel indicates 2nd week and the right panel indicates 3rd week of the assay. Gray bars indicate the colonies from cells expressing Intron sgRNA. Blue bars indicate colonies from cells expressing sgRNAs targeting Sgf29. n=3); ns=non-significant; *=P<0.05; **=P<0.005; ***=P<0.0005.

Fig. S4E: Effect of Sgf29 deletion on apoptosis in murine MLL-AF9 transformed leukemia. Immnoblot for PARP protein cleavage showing apoptosis in murine leukemia expressing Intron or Sgf29 targeting sgRNA. Two representative replicates are shown.

<u>Figure S5</u>

Fig. S5A: SDS-PAGE showing whole cell extract, cytoplasmic and ChEP-enriched fractions for NTC vs SGF29 knockout.

Fig. S5B: Heatmap of intensity changes in peptides for proteins evicted from the chromatin fraction of UB3 cells after SGF29 deletion in ChEP assay. R1, r2 and R3 are three independent replicates.

Figure S6

Fig. S6A: Heatmaps showing histone H3K9 acetylation (H3K9Ac) peaks centered around transcription start site (TSS) in UB3 cells transduced with non-targeting control (NTC) or SGF29 targeting sgRNA.

Figure S7

Fig. S7A: Cell cycle analysis in MLL-AF10 PDX cells after deletion of SGF29. A representative sample showing changes in different phases of cell cycle upon loss of SGF29 is shown here. Orange represents cells expressing non-targeting control (NTC) sgRNA whereas blue indicates the cells with SGF29 ko.

SUPPLEMENTARY METHODS

Epigenetic sgRNA library design

Our custom sgRNA library was designed based on a manually curated list of known epigenetic regulators, assigned to the following categories: regulators of chromatin reading, chromatin remodeling, DNA and RNA modification, histone acetylation and methylation, transcriptional elongation and other histone modifications. The gene list was then used directly as the input for the Broad Institute Genetic Perturbation Platform (GPP) sgRNA designer tool [210–213] to obtain 5 sgRNAs targeting early constitutive exons. To design sgRNAs targeting functional protein domains, we retrieved the coding sequences for ENSEMBL-annotated protein domains (GRCh37) using a custom script (cds_domain_finder.py). Non-targeting control sgRNAs were included in the design and represented ~5% of the total library size. The library sequences were synthesized on an array platform (Genscript, NJ) and then cloned into the lenti-guide Puro vector (Addgene: #52963, a kind gift from Dr. Feng Zhang, MIT) with the Gibson Assembly kit (New England Biolabs, NJ). The library plasmid was amplified using ElectroMAX™ Stbl4™ Competent Cells (Invitrogen, cat.11635018). The number of bacterial colonies was kept >500 times the number of sgRNA sequences in the library to maintain representation. To ensure the representation and identity of sgRNAs in the amplified pooled lentiviral plasmids, deep sequencing was performed on a HiSeq instrument (Illumina) and fastq files were analyzed using CRISPREssoCount [214]. The sgRNA sequences in these libraries are deposited as indicated in the data availability section.

Epigenetic CRISPR screen

The pooled epigenetics CRISPR library virus was produced using HEK293T cells transfected with Polyethylimine (PEI), pMD2.G, and psPAX2 as previously described [215]. 30 million UB3 cells were transduced with the pooled epigenetics library lentivirus in RPMI medium supplemented with 10% fetal bovine serum, antibiotics, and 8 μg/ml polybrene. The medium was changed 24 h after transduction to remove polybrene and cells were plated in fresh culture medium. 48 h after transduction, puromycin was added at a concentration of 1 μg/ml to select for cells transduced with the sgRNA library and then removed after 72 h. The virus titer was measured by infection of cells with serially diluted virus. To ensure transduction of a single sgRNA per cell, the multiplicity of infection (MOI) was set to 0.3 ~ 0.4. Adequate representation of sgRNAs during the screen

was ensured by keeping >1000x cells in culture relative to the library size. 10 million cells per replicate were harvested 3 days after puromycin removal for an initial time point (T0). Cells were FACS-sorted 5 days later to collect the upper and lower quartiles on the basis of GFP-expression using the FACSAria II Instrument (BD Biosciences) at the Sanford Burnham Prebys Flow Cytometry Core. Genomic DNA extraction from the T0 and GFP -low and -high cells was performed using the Zymo QuickDNA™ Midiprep Plus Kit (Zymo Research, Cat. D4068), according to the manufacturer's instructions. A two-step PCR-amplification for sequencing library preparation was conducted with TaKaRa Ex Taq™ Polymerase (TaKara, Cat. RR001) and custom primers to achieve adequate sequencing coverage in 1x75bp single-end reads, following published guidelines [214]. Barcoded libraries were pooled and sequenced using an Illumina Hiseq 500.

CRISPR competition experiments

To assess the candidate hits in independent assays, two top ranked individual sgRNAs from the sgRNA library were cloned for CSNK2A1, JADE3, AFF2, CCDC101, CSNK2B, DOT1L, ENY2, KAT7, KMT2A, MLLT1, and for non-targeting controls in the pKLV2-U6gRNA5(BbsI)-PGKpuro2ABFP-W vector (a gift from Kosuke Yusa, Addgene plasmid # 67974) [218] (sgRNA sequences provided in Table 2). Lentiviral supernatants were made from these constructs in a 96-well arrayed format. 10,000 UB3 cells were plated in a retronectin (Takara, #T202) coated flat bottom 96-well plate and transduced with the sgRNA viral supernatants by spinfection in polybrene-supplemented medium at an MOI of ~0.5. Cells were maintained in culture in 96-well plate format and assayed for proliferation every 3 days. A sample >10% of the culture volume was stained with SytoxRed (1:1000) (Thermo Fisher, # S34859) in PBS and monitored for the percentage of blue fluorescent protein (BFP) expressing cells progressively up to 21 days using high-throughput flow-cytometry [219].

Cell culture

Human leukemia cell lines U937 (Daniel Tenen, Beth Israel Deaconess Medical Center) and MOLM13 (ACC-554, DSMZ), were cultured in RPMI-1640 medium supplemented with 2 mM L-glutamine and sodium pyruvate, 10% Fetal bovine serum (FBS from… and 50 U/ml Penicillin/Streptomycin (Thermo Fisher Scientific, Carlsbad, CA), 2 mM L-glutamine and incubated in 5% CO2 at 37°C. Murine leukemia cells were cultured in DMEM medium supplemented with 2 mM L-glutamine, 15% FBS and 50U/ml Penicillin/Streptomycin, in the

presence of following cytokines: 10 ng/ml murine interleukin 6 (mIL-6), 6 ng/ml murine interleukin 3 (mIL3) and 20 ng/ml murine stem cell factor (mSCF) (all from Peprotech, Rocky Hill, NJ), and incubated at 5% CO2 and 37°C. HEK293T cells were cultured in DMEM medium supplemented with 2 mM L-glutamine and sodium pyruvate, 10% FBS and 50 U/ml Penicillin/Streptomycin, and incubated in 5% CO2 at 37°C. MLL-AF10 patient derived xenograft (PDX) cells were cultured in IMDM medium supplemented with 20% BIT9500 (STEMCELL Technologies), human cytokines and StemRegenin 1 44 (SR1) and UM171 as described earlier(11).

Generation of murine reporter leukemia

For mouse experiments, inducible MLL-AF9 murine leukemias were generated in lineage-depleted bone marrow cells of mice with a *GFP-Meis1* (12) or *CAG-Cas9* (13) background. Hematopoietic stem and progenitor cells (HSPCs) were isolated from bone marrow of C57Bl/6 mice using EasySep lineage depletion (STEMCELL Technologies) kit. HSPCs were cultured over-night in DMEM medium supplemented with 15% FBS and mSCF, mIL6 and mIL3 in a 37 °C incubator with 5% CO_2. The following day, the cells were transduced with viral supernatants containing the MSCV-MLL-AF9-neo and the MSCV-rTTA-2A-BFP constructs by spinfection at 2500 rpm at 30°C for 90 min. 72 hr post-transduction, BFP+ve cells were sorted using the FACSAria II (BD Biosciences) flow cytometer (11). *In vitro* transformed BFP+ cells were then injected into sub-lethally irradiated C57Bl/6 recipient mice from the SBP Animal vivarium to generate primary leukemias.

Small-molecule library composition and design

265 small-molecule inhibitors targeting diverse classes of epigenetic regulators were manually curated and purchased from various commercial sources by the Conrad Prebys Center for Chemical Genomics (Table S1).

Flow-cytometry-based small-molecule screen

Compounds were dispensed with the Labcyte Echo 555 (Labcyte Inc., Sunnyvale, CA) acoustic droplet ejection dispenser to a final concentration of 0.11 μM and 10 μM, in technical triplicates. Human UB3 cells were then seeded in 384-well plates (PerkinElmer Health Sciences, Inc.) with a MicroClime® lid (Labcyte Inc.) at a density of 2,000 cells per well in 45 μl of culture medium

using the Multidrop™ Combi Reagent Dispenser (ThermoFisher Scientific). Cells were incubated for 5 days at 37 ºC, 5% CO2 and 95% humidity, and 5 µl of Sytox Red viability stain was then added to the culture volume using the Multidrop™ Combi Reagent Dispenser. High throughput flow cytometry was performed in the HTS unit of the Fortessa 14-color (BD) at the SBP Flow Cytometry Core. Flow cytometry data was analyzed with Flowjo version 10.0.4 (Flowjo LLC).

Quantitative RT-PCR

The mRNA levels were measured by real time quantitative PCR (RT-qPCR) using standard protocols. RNA was extracted using the RNA extraction kit (Qiagen, Hilden, Germany) and was used to synthesize cDNA with the Protoscipt® II First Strand cDNA Synthesis Kit (New England Biolabs Inc., Beverly, MA). For PCR-based amplification, cDNA and primers were added to the SYBR Green PCR Master mix (ThermoFisher, Carlsbad, CA). Expression levels for *HOXA7,HOXA9, HOXA10, MEIS1, GAPDH and HPRT* were determined with the oligo sequences listed in Table S4 and measured on the Stratagene MX3000P (Agilent Technologies). Relative quantity of mRNA was determined by the ΔΔCT method as previously described [150] using HPRT as the internal reference.

Colony formation assays

For murine leukemia colony forming cell (CFC) assays, CALM-AF10, MLL-AF9, and MLL-AF10 lines were transduced with retroviral particles encoding 2 sgRNAs targeting Sgf29 exon sequences and one sgRNA targeting an intronic sequence of Sgf29 as a control (sequences provided in Table S4), cloned in pMSCV-U6sgRNA(BbsI)-PGKpuro2ABFP (a gift from Sarah Teichmann, Addgene #102796). Cells were transduced by spinfection as described above and cultured for 48 hours in the 37 °C incubator with 5% CO_2. Puromycin (2.5 µg/ml) was then added to the cultures for 48 hours to select for puromycin resistant cells. 1000 cells were plated in 35 mm dish, in duplicates, in 1mL Methylcellulose-based MethoCult M3234 medium (STEMCELL Technologies) supplemented with 10 ng/ml mIL6, 6 ng/ml mIL3 and 20 ng/ml mSCF (Peprotech) and colonies were scored on day 7. After scoring, colonies were washed with PBS, pooled, and counted for subsequent replating. A sample was taken for cell morphology assessment, performed by spinning 100,000 cells resuspended in 150 µl PBS onto glass slides, using the Cytospin 4 cytocentrifuge (Thermo Scientific) followed by Wright-Giemsa staining. Cells were replated every week for 3 weeks at the same cell number to test secondary and tertiary replating potential. For colony assays with Lin- Sca+ c-Kit+ (LSK) murine cells, bone marrow cells from

Cas9 transgenic mice (13) were lineage-depleted using the EasySep lineage depletion kit (STEMCELL Technologies) to obtain a lineage negative (Lin-) population. Lin- cells were then stained with the following antibodies: FITC- conjugated Streptavidin (eBioscience), Pacific Blue-conjugated Sca-1 (Biolegend, San Diego, CA), and Alexa647-conjugated cKit (Biolegend, San Diego, CA) and sorted for the Lin- Sca-1+ cKit+ (LSK) population using the FACSAria II cytometer (BD Biosciences). Cells were kept in culture overnight and transduced the following day with retroviral particles with sgRNAs targeting Sgf29 and an intron control, as described above. The cells were counted and plated for colony formation in M3434 methylcellulose-based media (STEMCELL Technologies) at a concentration of 10,000 cells per ml, as described above. Colonies were scored on day 10.

Dye-dilution experiments

To trace cell proliferation by flow cytometry, MOLM13 and U937 cells were transduced by spinfection with lentiviral particles containing sgRNAs targeting SGF29 or non-targeting controls (refer to Table S4), cloned in lentiGuide-Puro vector (a gift from Feng Zhang, Addgene #52963). Then, cells were incubated overnight and treated with 1 μg/ml puromycin for 3 days. Upon selection, the cells were washed and stained with the CellTrace™ Violet dye (ThermoFisher Scientific), according to the manufacturer's instructions. Cells were maintained in culture in the dark and a sample (>10% of culture volume) was assayed every day for 6 days by flow cytometry.

Viral preparation, transduction and selection

Lentivirus was made from the CROP-seq pooled DNA by transfection of the CROP-seq pool together with Polyethylimine (PEI), pMD2.G, and psPAX2 in HEK293T cells, as described previously [215]. Viral supernatants were collected at 48 and 72 hours post-transfection, and then filtered (0.45 μm) and pooled. Viral supernatants were then concentrated by centrifugation (20,000 rpm, 2 hrs, 4° C) and used for transduction of UB3 cells by incubation with 0.8 μg/μl of polybrene overnight. Medium was changed after overnight incubation. At 48h post-transduction, puromycin (1μg/μl) was added to cell suspensions for 3 days of selection. Cells were pelleted for sequencing 3 days after removal of puromycin.

Single cell sequencing

Two independently transduced samples were sequenced for the CROP-Seq experiment. Cell concentration and viability was assessed using a hemocytometer and viability for all samples was > 80%. A total of 18,000 cells per sample were loaded on a Chromium Single Cell Instrument (10x Genomics, Pleasanton, CA). RNAseq libraries were prepared using the Chromium Single Cell 3′ v3.1 Library, Gel Beads & Mutiplex Kit (10x Genomics). CDNA was PCR-amplified and purified using SPRIselect Reagent Kit (Beckman Coulter). Sequencing was performed on the Illumina NovaSeq using the S4 200 kit and PE100 run configuration at the University of California San Diego Center for Epigenomics. Cell Ranger Single-Cell Software Suite (v4.0.0; 10x Genomics) was used for sample demultiplexing, alignment, filtering, and UMI counting.

CROP-seq data analysis

sgRNAs were detected in the fastq files via a custom script, which required a perfect match for either the 10bp upstream or 10bp downstream of the sgRNA, as well as the sgRNA sequence with at most 1 mismatch. If a partial sgRNA was located at the end of a sequence but at least 10bp matched a unique sgRNA (along with the correct neighboring sequence), the read was counted as well (CropSeq_sgRNA_from_ fastq.cpp).

10X fastq reads were trimmed using trim-galore (v0.6.6, flags -a AAAAAAAAAAAA --length 10) which relies on cutadapt (v2.5). Reads were aligned to the genome (hgGRCh38) using STAR (v2.7.3a). All multimapping reads were removed (samtools view -b -q 254), and reads were deduplicated by UMI using custom code (CropSeq_10x_Remove_Duplicates.cpp). Reads were then mapped to genes using bedtools v2.29.2. Reads spanning exon boundaries were split (-split flag used), and all reads were first mapped to exons (flags -f 0.95 -c 7 -o distinct) and then mapped to genes (-f 0.95 -c 4 -o distinct), such that a read mapping to overlapping genes is preferentially assigned to the gene in which it overlaps an exon. Cells with fewer than 10^3.5 (3162) UMIs or fewer than 200 expressed genes, or whose barcodes were not on the 10x barcode whitelist were removed. Cells with more than one gRNA were also removed. Finally, genes present in fewer than 3 cells were not included in downstream analyses. General processing and evaluation of sgRNA target gene expression, was performed in R (CROPSeq_HOX.R). All plots in Figure 24 were generated in R (CROPSeq_HOX.R). UMAP and ridgeplots were generated using the Seurat

package. The dendrogram was generated using the R function dist(method = "euclidean") and hclust(method = "ward.D2"). The heatmap was generated using the pheatmap package.

RNA-sequencing

U937-MEIS1-GFP and MOLM13 cells were plated at a density of 1 million cells per ml in T75 tissue culture flasks and transduced in triplicates with sgRNAs for non-targeting controls or SGF29. Cells were selected with puromycin as described above. 2 million cells were harvested at 7 days post-selection from every replicate and RNA was extracted using the RNeasy Mini kit (Qiagen, Hilden, Germany). RNA-seq Libraries were prepared using NEBNext Ultra II Directional RNA Library Prep Kit (New England Biolabs, Ipswich, MA) for Illumina as per the manufacturer's protocol. For each sample, 900 ng of total RNA was amplified in 10 cycles of PCR amplification. Sequencing was performed to obtain 1x75bp reads on the Illumina NextSeq500 by the Genomics core at SBP Medical Discovery Institute. Next-generation sequencing data were demultiplexed and processed with the Illumina Basespace RNA-Seq Differential Expression Analysis workflow.

RNA-sequencing data analysis

Raw reads were preprocessed by trimming Illumina Truseq adapters, polyA, and polyT sequences using cutadapt v2.3[226] with parameters "cutadapt -j 4 -m 20 --interleaved -a AGATCGGAAGAGCACACGTCTGAACTCCAGTCAC -A AGATCGGAAGAGCGTCGTGTAGGGAAAGAGTGT Fastq1 Fastq2 | cutadapt --interleaved -j 4 -m 20 -a "A{100}" -A "A{100}" - | cutadapt -j 4 -m 20 -a "T{100}" -A "T{100}" -". Trimmed reads were subsequently aligned to human genome version hg38 using STAR aligner v2.7.0d_0221 [227] with parameters according to ENCODE long RNA-seq pipeline (https://github.com/ENCODE-DCC/long-rna-seq-pipeline). Gene expression levels were quantified using RSEM v1.3.1 [228]. Ensembl v84 gene annotations were used for the alignment and quantification steps. RNA-seq sequence, alignment, and quantification qualities were assessed using FastQC v0.11.5 (https://www.bioinformatics.babraham.ac.uk/projects/fastqc/) and MultiQC v1.8 [229]. Lowly expressed genes were filtered out by retaining genes with estimated counts (from RSEM) ≥ number of samples times 5. Filtered estimated read counts from RSEM were used for differential expression comparisons using the Wald test implemented in the R Bioconductor package DESeq2 v1.22.2 based on generalized linear model and negative binomial distribution [230](Love, Huber et al. 2014). Genes with Benjamini-Hochberg corrected p-value < 0.05 and fold change ≥ 2.0 or ≤ 2.0 were selected as differentially expressed genes. Pathway analyses of differential

expression comparisons were performed using Ingenuity Pathway Analysis (Qiagen, Redwood City, USA).

Chromatin immunoprecipitation and sequencing (ChIP-Seq)

UB3 cells expressing Cas9 were transduced with sgRNAs for a non-targeting control or SGF29, as described for the dye-dilution experiment. Chromatin immunoprecipitation was performed as previously described [150]. Cells were fixed with 1% formaldehyde and chromatin was sheared using a Bioruptor™ (Diagenode Inc, NJ) in 15 cycles (each one in high-setting for 30 s on and 30 s off), at 4°C. Chromatin was immunoprecipitated using antibodies for normal rabbit IgG (Cell Signaling Technology, Cat. No, 2729) and Histone H3K9ac (Abcam, ab4441). For SGF29 binding studies, U937 cells transduced with 3x Flag tagged SGF29 wt or D196R mutant viral supernatants were fixed with 1% formaldehyde for 15 minutes and chromatin was sheared as described earlier. Chromatin was immunoprecipitated using Anti-FLAG M2 affinity beads (Sigma Aldrich, #A2220). Library preparation on eluted DNA was performed using the NEBNext Ultra II DNA library prep kit for Illumina (E7645S and E7600S) as per the manufacturer's protocol. DNA libraries were sequenced in paired-end 150 bp reads in a NovaSeq600 sequencer (Illumina, San Diego, CA) by Novogene Corporation (Sacramento, CA).

Chromatin enrichment for proteomics (ChEP)

Five million U937 cells were transduced in 4 replicates with concentrated lentiviral supernatants containing a non-targeting control or sgRNAs targeting CSNK2A1 or SGF29 in the pKLV2-U6gRNA5(BbsI)-PGKpuro-2ABFP backbone (a gift from Kosuke Yusa, Addgene #67974; see Table 2 for sequences). 48 hours after transduction, cells were treated with 1 μg/ml puromycin for 3 days. The cultures were grown for 7 days and counted for chromatin enrichment for proteomics procedure [231]. Briefly, 100 million cells per replicate were collected by centrifugation for 5 minutes at 600 xg at room temperature and washed with pre-warmed PBS. Cells were then resuspended in 1% formaldehyde in pre-warmed PBS and incubated for 10 min at 37°C in a rotator. Crosslinking was halted by adding glycine to a final concentration of 0.25M and incubating for 5 min at room temperature in a rotator. Cells were then washed with pre-warmed PBS and pellets were collected by centrifugation at room temperature for 5 min at 600 xg and stored at -80 °C. Pellets were thawed and resuspended in 1 ml cold cell lysis buffer (25 mM Tris, 0.1% Triton X-100, 85 mM KCl, and protease inhibitors), transferred to 2 ml tubes, and homogenized carefully

with a 200 µl pipette tip. The samples were then centrifuged for 2300 xg for 5 min at 4°C and the supernatants containing the cytoplasmic fraction were recovered and stored at -80°. The nuclei pellets were resuspended in 500 µl cell lysis buffer containing 200µl/ml RNAse A and were incubated for 15 min at 37°C. Samples were then kept on ice and centrifuged at 2,300 xg for 10 min at 4 °C. The supernatants were then discarded, and pellets were resuspended in 500 µl SDS buffer (50 mM Tris, 10 mM EDTA, 4% SDS, and protease inhibitors) with 200 µl pipette tips and incubated for 10 min at room temperature. Samples were then centrifuged at 16,000 xg for 30 min at room temperature and the supernatants were discarded. The pellets were washed by resuspending in 500 µl SDS buffer with a 200 µl tip, then adding 1.5 ml urea buffer (10 mM Tris, 1 mM EDTA, and 8 M urea) and mixing by inversion several times. The tubes were then spun down at 16,000 xg for 25 min at room temperature and supernatants were discarded. Urea was washed out by resuspending in 500 µl SDS buffer with a 200 µl tip, then adding 1.5 ml SDS buffer and mixing by inversion several times. The tubes were spun down at 16,000 xg for 25 min at room temperature and the pellets were covered with storage buffer (10 mM Tris, 1mM EDTA, 25 mM NaCl, 10% glycerol, and protease inhibitors) and flicked to dislodge the pellets. The pellets were transferred to Bioruptor® shearing tubes (Diagenode Inc, Denville, NJ) and sonicated in a Bioruptor® (Diagenode Inc., Denville, NJ) for 15 min in 15 cycles (each 30 s on, 30 s off on high-intensity setting). The samples were centrifuged at 16,000 xg for 30 min at 4 °C and the supernatants were transferred to a new tube and stored at -80 °C for mass spectrometry analysis.

LC-MS/MS analysis

For the chromatin-enriched for proteomics samples, 30 µg of each sample were processed using the ProTiFi S-trap™ digestion system. Mass spectrometry data were acquired on an Orbitrap Exploris 480 (ThermoFisher, Bremen, Germany) instrument at the Cedars Sinai Proteomics and Metabolomics Core in the Advanced Clinical Biosystems Research Institute. Desalted peptides were separated on an Ultimate 3000 ultra-high-pressure chromatography system with a 60-min gradient. Peptides were separated on a gradient of 1% B organic phase for 2 minutes, 1-5% B for 0.5 minutes, 5-9% B for 3.5 minutes, 9-27% B for 39 minutes, and 27-44% B for the final 15 minutes on a C18 column (15 cm length, 300 µm diameter) at a flow rate of 9.5 nL/min. Source parameters included spray voltage at 3 kV, capillary temp of 300 °C , and RF funnel level of 40%. MS1 resolutions were set to 60,000 and AGC was set to “standard” with ion transmission of 100ms. Mass range of 400-1000 and AGC target value for fragment spectra of 300% were used. Peptide ions were fragmented at a normalized collision energy of 30%. Fragmented ions were detected across 50 DIA windows of 12 Da. MS2 resolutions were set to 15,000 with an ion

transmission time of 25 ms. All data were acquired in profile mode using positive polarity. The data were searched using the DIA-NN tool against a human in silico digested sequence reference library.

Data analysis for ChEP

Protein peak data (mz/rt) were analyzed using MetaboAnalyst 5.0. Missing values were imputed by replacing them with 1/5th of the minimum positive values of their corresponding variables. No data filtering was applied. Important features were selected based on fold change analysis with a threshold of 2 and t-test P. values below 0.05.

Western and dot blotting

Whole cells were lysed in cold RIPA buffer containing the Halt™ protease inhibitor cocktail for 30 min on ice (ThermoFisher Scientific, Carlsbad, CA). Protein supernatant was collected after 30 min of 12,000 rpm centrifugation at 4°C and stored at -80°C until use. Protein concentrations from whole cell lysates were determined using the Pierce™ BCA protein assay kit (ThermoFisher Scientific). For the immunoblotting, the following antibodies were used: KAT2A (Abcam, ab217876), Flag M2 (Sigma-Aldrich, F1804), Vinculin (Sigma-Aldrich, V9131), H3 (Abcam, ab1791), and SGF29 (Abcam, ab204367). Protein samples (50µg total protein) were resolved by SDS-PAGE using 4-12% Bis-Tris Bolt™ gels (Invitrogen, NW04120BOX) and transferred to iBlot2™ nitrocellulose membranes (ThermoFisher Scientific, IB23002). The membranes were blocked with 5% non-fat milk in Tris-buffered Saline containing 0.01% tween-20 (0.01% TBST). The membranes were probed with species-specific goat anti-rabbit (MilliporeSigma, AP307P) or goat anti-mouse (ThermoFisher Scientific, 31446) HRP-conjugated secondary antibody and detected with enhanced chemiluminescence (ECL) detection kit (Thermo Fisher, Carlsbad, CA).

Cell Cycle Analysis

500,000 MLL-AF10 PDX cells expressing NTC or SGf29 sgRNA were washed with cold PBS and fixed with chilled 70% ethanol. Fixed cells were incubated at -20°C for 1 hr. Cells were then centrifuged at 2000 rpm for 3 min. at 4°C. Pellets were resuspended in PBS containing RNAse A and Propidium Iodide (PI) and incubated at 37°C for 30 min. in dark and analysed using flow cytometry.

REFERENCES

1. Doench JG, Fusi N, Sullender M, Hegde M, Vaimberg EW, Donovan KF, et al. Optimized sgRNA design to maximize activity and minimize off-target effects of CRISPR-Cas9. Nat Biotechnol. Nature Publishing Group; 2016;34:184–91.

2. Sanson KR, Hanna RE, Hegde M, Donovan KF, Strand C, Sullender ME, et al. Optimized libraries for CRISPR-Cas9 genetic screens with multiple modalities. Nat Commun. Nature Publishing Group; 2018;9:1–15.

3. Kim HK, Min S, Song M, Jung S, Choi JW, Kim Y, et al. Deep learning improves prediction of CRISPR-Cpf1 guide RNA activity. Nat Biotechnol. 2018;36:239–41.

4. DeWeirdt PC, Sanson KR, Sangree AK, Hegde M, Hanna RE, Feeley MN, et al. Optimization of AsCas12a for combinatorial genetic screens in human cells. Nat Biotechnol [Internet]. 2020; Available from: https://www.ncbi.nlm.nih.gov/pubmed/32661438

5. Canver MC, Haeussler M, Bauer DE, Orkin SH, Sanjana NE, Shalem O, et al. Integrated design, execution, and analysis of arrayed and pooled CRISPR genome-editing experiments. Nat Protoc. 2018;13:946–86.

6. Joung J, Konermann S, Gootenberg JS, Abudayyeh OO, Platt RJ, Brigham MD, et al. Genome-scale CRISPR-Cas9 Knockout and Transcriptional Activation Screening. Nat Protoc. 2017;12:828–63.

7. Li W, Köster J, Xu H, Chen CH, Xiao T, Liu JS, et al. Quality control, modeling, and visualization of CRISPR screens with MAGeCK-VISPR. Genome Biol. 2015;16:281.

8. Wang B, Wang M, Zhang W, Xiao T, Chen CH, Wu A, et al. Integrative analysis of pooled CRISPR genetic screens using MAGeCKFlute. Nat Protoc. 2019;14:756–80.

9. Tzelepis K, Koike-Yusa H, De Braekeleer E, Li Y, Metzakopian E, Dovey OM, et al. A CRISPR Dropout Screen Identifies Genetic Vulnerabilities and Therapeutic Targets in Acute Myeloid Leukemia. Cell Rep. 2016;17:1193–205.

10. Deshpande A, Chen BR, Zhao L, Saddoris K, Kerr M, Zhu N, et al. Investigation of Genetic Dependencies Using CRISPR-Cas9-based Competition Assays. J Vis Exp [Internet]. 2019; Available from: https://www.ncbi.nlm.nih.gov/pubmed/30663717

11. Chen B-R, Deshpande A, Barbosa K, Kleppe M, Lei X, Yeddula N, et al. A JAK/STAT-mediated inflammatory signaling cascade drives oncogenesis in AF10-rearranged AML. Blood. American Society of Hematology; 2021;137:3403–15.

12. Xiang P, Wei W, Hofs N, Clemans-Gibbon J, Maetzig T, Lai CK, et al. A knock-in mouse strain facilitates dynamic tracking and enrichment of MEIS1. Blood Adv. 2017;1:2225–35.

13. Platt RJ, Chen S, Zhou Y, Yim MJ, Swiech L, Kempton HR, et al. CRISPR-Cas9 knockin mice for genome editing and cancer modeling. Cell. Elsevier BV; 2014;159:440–55.

14. Deshpande AJ, Deshpande A, Sinha AU, Chen L, Chang J, Cihan A, et al. AF10 Regulates Progressive H3K79 Methylation and HOX Gene Expression in Diverse AML Subtypes. Cancer Cell [Internet]. 2014; Available from: http://dx.doi.org/10.1016/j.ccell.2014.10.009

15. Datlinger P, Rendeiro AF, Schmidl C, Krausgruber T, Traxler P, Klughammer J, et al. Pooled CRISPR screening with single-cell transcriptome readout. Nat Methods. 2017;14:297–301.

16. Martin M. Cutadapt removes adapter sequences from high-throughput sequencing reads. EMBnet J. EMBnet Stichting; 2011;17:10.

17. Dobin A, Davis CA, Schlesinger F, Drenkow J, Zaleski C, Jha S, et al. STAR: ultrafast universal RNA-seq aligner. Bioinformatics. Oxford University Press (OUP); 2013;29:15–21.

18. Li B, Dewey CN. RSEM: accurate transcript quantification from RNA-Seq data with or without a reference genome. BMC Bioinformatics. Springer Science and Business Media LLC; 2011;12:323.

19. Ewels P, Magnusson M, Lundin S, Käller M. MultiQC: summarize analysis results for multiple tools and samples in a single report. Bioinformatics. Oxford University Press (OUP); 2016;32:3047–8.

20. Love MI, Huber W, Anders S. Moderated estimation of fold change and dispersion for RNA-seq data with DESeq2. Genome Biol. Springer Science and Business Media LLC; 2014;15:550.

21. Kustatscher G, Wills KLH, Furlan C, Rappsilber J. Chromatin enrichment for proteomics. Nat Protoc. Springer Science and Business Media LLC; 2014;9:2090–9.